Vortices in Photon Bose-Einstein Condensates

Diploma Thesis of

Joshua Krauß

RPTU Rheinland-Pfälzische Technische Universität Kaiserslautern Landau

RP TU Rheinland-Pfälzische Technische Universität Kaiserslautern Landau

Vortices in Photon Bose-Einstein Condensates

Diplomarbeit in Theoretischer Physik

durchgeführt von

Joshua Krauß

am Fachbereich Physik der
RPTU Kaiserslautern-Landau

unter Anleitung von

Priv.-Doz. Dr. Axel Pelster

December 5, 2023

Abstract

Since A. Einstein's prediction of the existence of a Bose-Einstein condensate, in which the ground state of a bosonic gas is macroscopically occupied below a critical temperature. The experimental realisation was achieved by W. Ketterle in a ^{23}Na gas and by C. Wieman and Cornell for ^{87}Rb, Bose-Einstein condensates have been extensively studied. One of the most exciting Bose-Einstein condensates in the last 10 years is a condensate of photons. This basically consists of a microresonator filled with dye molecules. On the one hand, the resonator ensures that the photons are harmonically trapped and, on the other hand, the interaction of the photons with the dye ensures that the photons interact effectively with each other and more import thermalize at room temperature. Due to the nature of the system, photons can leave the condensate, which must be compensated for by constantly adding photons. Thus, a photon Bose-Einstein condensate is a prime example of an open dissipative system.
A fascinating phenomenon in Bose-Einstein condensates are vortices, which reflect topological defects in the flow of a quantum fluid. An essential part of the theoretical description of vortices is the velocity field caused by the presence of the defects, which changes depending on the system under consideration. Thus, the velocity field of a single vortex in a closed system consists of circular streamlines, whereas in an open dissipative system spiral streamlines become visible.
The main part of this thesis is the construction of a method to analytically find approximate solutions of an arbitrary equation of motion underlying the system. The basic principle is to approximate the wave function of the system by a suitable ansatz depending on different parameters and then to determine these parameters by projecting the equation of motion onto the chosen parameter manifold.
Equipped with this method, we then consider an open dissipative system, which is described by a Gross-Pitaevskii equation generalised to open dissipative systems, and apply the constructed projection optimization method to various systems for which only numerical solutions are currently available. Thus, we compute approximate analytical solutions for an open dissipative condensate in a harmonic trap. The special feature thereby is that the density profile of the condensate changes significantly depending on the system parameters used for pumping and losses due to the generation of supercurrents. Furthermore, we consider an infinitely extended condensate without external trapping potential in the presence of a single vortex. Using the projection optimization method, we construct an analytical solution of the velocity field and thus achieve the description of the spiral shape.

Zusammenfassung

Seit der Vorhersage A. Einsteins der Existenz eines Bose-Einstein Kondensats, bei dem der Grundzustand eines Bosonen Gases unterhalb einer kritischen Temperatur makroskopisch besetzt wird; und der experimentellen Realisierung durch W. Ketterle in einem ^{23}Na Gas bzw. durch C. Wieman für ^{87}Rb wurden Bose-Einstein Kondensate ausführlich untersucht. Eines der wohl spannendsten Bose-Einstein Kondensate in den vergangenen 10 Jahren ist ein Kondensat aus Photonen. Dieses besteht grundlegend aus einem Mikroresonantor gefüllt mit Farbstoffmolekülen. Dabei sorgt zum einen der Resonator dafür, dass die Photonen harmonisch gefangen werden, und zum anderen die Interaktion der Photonen mit dem Farbstoff für eine effektive Wechselwirkung der Photonen untereinander und noch wichter für die Thermalisierung bei Raumtemperatur. Aufgrund der Beschaffenheit des Systems können Photonen das Kondensat verlassen, das durch ständiges Hinzufügen von Photonen kompensiert werden muss. Somit ist ein Photonen Bose-Einstein Kondensat ein Paradebeispiel für ein offen dissipatives System.
Ein faszinierendes Phänomen in Bose-Einstein Kondensaten sind Vortizes, welche topologische Defekte im Fluss einer Quantenflüssigkeit widerspiegeln. Ein essenzieller Teil in der theoretischen Beschreibung von Vortizes ist dabei das durch die Anwesenheit der Defekte verursachte Geschwindigkeitsfeld, welches sich abhängig vom betrachteten System verändert. So besteht das Geschwindigkeitsfeld eines einzelnen Vortex in einem abgeschlossenes System aus kreisförmigen Stromlinien, wohingegen in einem offen dissipativen System spiralförmige Stromlinien sichtbar werden.
Der Hauptbestandteil dieser Arbeit ist die Konstruktion eines Verfahrens, um approximativ Lösungen einer beliebigen, dem System zugrundliegenden, Bewegungsgleichung analytisch zu finden. Das Grundprinzip dabei besteht darin, die Wellenfunktion des Systems durch einen geeigneten Ansatz abhängig von verschiedenen Parametern zu nähern und anschließend die Parameter durch Projektion der Bewegungsgleichung in eine Mannigfaltigkeit zu bestimmen.
Mit dieser Methode ausgestattet betrachten wir anschließend ein offen dissipatives System, welches beschrieben wird durch eine entsprechend auf offen dissipative Systeme verallgemeinerte Gross-Pitaevskii Gleichung, und wenden die konstruierte Projektions Optimierungs Methode auf verschiedene Systeme an, bei denen aktuell nur numerische Lösungen vorliegen. Damit berechnen wir approximative analytische Lösungen für ein offen dissipatives Kondensat in einer harmonischen Falle. Dabei liegt die Besonderheit darin, dass sich das Dichteprofil des Kondensats abhängig von der verwendeten Systemparametern für Pumpen und Verluste durch die Erzeugung von Superströmen stark verändert. Außerdem betrachten wir ein unendlich ausgedehntes Kondensat ohne äußeres Fallenpotential in Anwesenheit eines einzelnen Vortex. Mit Hilfe des Proektionsverfahrens konstruieren wir eine analytische Lösung des Geschwindigkeitsfeldes und erreichen damit die Beschreibung der Spiralform.

Contents

1. Introduction **1**
- 1.1. Atomic Quantum Gases . . . 1
- 1.2. Photon Bose-Einstein Condensates . . . 2
  - 1.2.1. Experimental Setup . . . 2
  - 1.2.2. Theoretical Foundations . . . 4
- 1.3. Vortices in Quantum Gases . . . 4
  - 1.3.1. Vortices in Closed Systems . . . 4
  - 1.3.2. Vortices in Open Dissipative Systems . . . 5
- 1.4. Outline . . . 7

2. Mean-Field Model of Interacting Bose Gas in BEC Phase **8**
- 2.1. The Gross-Pitaevskii Equation . . . 8
- 2.2. The Complex Gross-Pitaevskii Equation . . . 10
  - 2.2.1. Heuristical Derivation . . . 10
  - 2.2.2. Linear Stability Analysis . . . 11

3. Hydrodynamic Description **15**
- 3.1. Closed System . . . 15
  - 3.1.1. Hydrodynamic Equations in 3D . . . 16
  - 3.1.2. Hydrodynamic Equations in 2D . . . 17
- 3.2. Open dissipative System . . . 20
  - 3.2.1. Hydrodynamic Equations in 3D . . . 20
  - 3.2.2. Hydrodynamic Equations in 2D . . . 21

4. Optimization Methods **23**
- 4.1. Least Action Optimization Method . . . 23
- 4.2. Cumulant Method . . . 24
- 4.3. Projection Optimization Method . . . 25

5. Non-Vortex Solution **27**
- 5.1. Projection Optimization Solution . . . 27
- 5.2. Cumulant Solution . . . 30
- 5.3. Solution With Complex Phase . . . 32

6. Vortex Solution **35**
- 6.1. Closed System . . . 35
  - 6.1.1. Least Action Variational Method vs. Projection Optimization Method . . . 35

6.1.2. Alternative Optimization Ansatzes 37
6.1.3. Discussion 39
6.2. Open Dissipative System 40
6.3. Discussion and Numerical Simulation 45

7. Continuum Model **52**

8. Summary and Outlook **56**

A. Projection Optimization Method **58**

B. Useful Integrals **60**
B.1. Exponential Ansatz 60
B.2. Hyperbolic Tangens Ansatz 61

Bibliography **64**

1. Introduction

The field of ultracold quantum gases in open-dissipative systems has become better known in the last ten years. In particular, the experimental realization of a Bose-Einstein condensate from pure light in 2010 attracted a a lot of attention. One challenge here is the description of vortices. This thesis is devoted to the theoretical modelling of an open-dissipative Bose-Einstein condensate of light, taking into account also the existence of a vortex. As an introduction to the topic, this chapter first gives a historical overview of Bose-Einstein condensation. The experimental and theoretical foundations of a condensate of light are then presented, followed by a brief introduction to vortices, starting with atomic Bose-Einstein condensates and moving on to condensates of photons.

1.1. Atomic Quantum Gases

Atomic quantum gases represent a fascinating area at the forefront of modern physics, where matter behaves in extraordinary ways dictated by the laws of quantum mechanics. These gases consist of collections of ultracold atoms that, when cooled to temperatures close to absolute zero, undergo a remarkable phase transition, revealing their quantum nature.
One of the occurring macroscopic quantum phenomena in bosonic gases is the Bose-Einstein condensation (BEC), where the single particles loose their individual identities and occupy a single quantum state, the quantum mechanical ground state. The foundation of Bose-Einstein condensation is based on theoretical considerations by A. Einstein in 1925 [1] based on the work of Bose in 1924 [2] on the statistics of photons. Einstein considered a non-interacting, massive Bose gas and came to the conclusion that there must be a phase transition. This phase transition is characterized by the fact that below a critical temperature, the state with the lowest energy is occupied by a macroscopic number of atoms.
However after Einsteins claim it took over one decade to become practically important. Only with the discovery of superfluidity in liquid helium by Allan and Misener in 1938 [3] and the resulting thoughts on linking superfluidity and BEC of London in the same year [4] brought more attention. To see the connection, London calculated the critical temperature for Bose-Einstein condensation ($T_c = 3.1\text{K}$) and the lambda point ($T_\lambda = 2.17\text{K}$) at which ^{4}He becomes a superfluid [5]. As these two temperatures are very close to each other, a connection was suspected. Indeed superfluid liquid helium is the prototype of a BEC, but due to strong atomic interactions the number of condensed atoms is drastically reduced such that it was difficult in 1938 to measure the real occupation of the ground state.

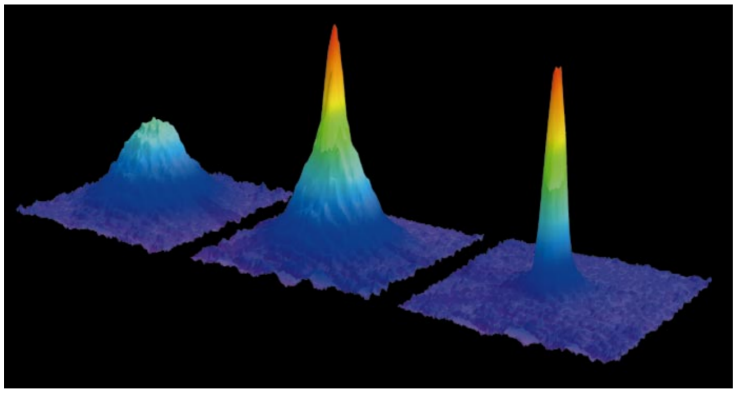

Figure 1.1.: Creation of a BEC. Left: Cooled Bose gas right above critical temperature. Middle: Beginning of condensation right after critical temperature. Right: BEC after further cooling. Taken from [8].

This was the reason why many experimental physicists then concentrated to generate a BEC for dilute Bose gases. Only after achieving the technique of laser cooling various BEC's for different atom gases were produced in 1995 by Cornell and Wieman [6] for ^{87}Rb or by Ketterle [7] for ^{23}Na, see also Fig. 1.1.

Today the concept of Bose-Einstein condensation is applied to many more systems different to liquid helium. Even for a system without energy conservation like exciton-polaritons or photons it is also possible to reach condensation. This leads directly to the next section.

1.2. Photon Bose-Einstein Condensates

The first condensate of light was not a condensate of pure light, but a nonequilibrium condensate of exciton-polaritons [9–11]. These are condensates of quasi-particles, which are built up of electron-hole pairs and cavity photons.
The first pure photon condensate was realised by the Weitz group in 2010 [12] and is usually prohibited by the lack of particle conservation. In the following we provide an overview on the experimental realization and the theoretical description of a Photon Bose-Einstein condensate (PBEC).

1.2.1. Experimental Setup

The experimental realisation of a photon Bose-Einstein condensate essentially requires two main components. Firstly, thermal equilibrium and secondly, a cavity. To reach thermal equilibrium and therefore doing the first step in realizing a BEC it is usually crucial to have a particle-particle interaction, which is realized for photons by coupling them to a bath of dye molecules. Due to the lack of such a direct interaction for photons one uses an optical microcavity filled with dye-molecules, sketched in Fig. 1.2 (a). In the experiment typically the dye Rhodamine 6G is

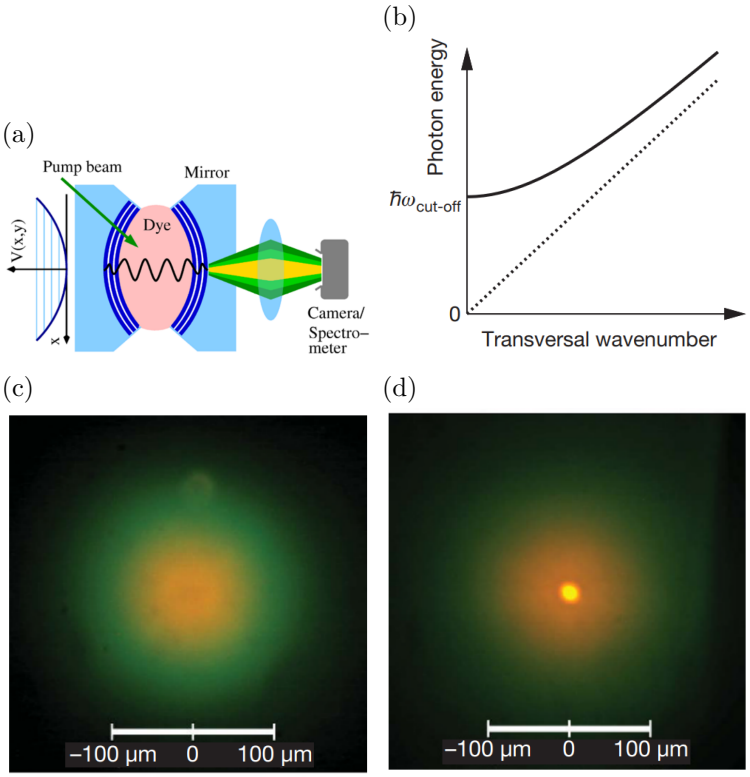

Figure 1.2.: (a) Sketch of experimental setup; (b) Dispersion relation of the photonic modes; (c) Image of the spatial photon distribution transmitted through one mirror below threshold; (d) above threshold showing the condensation. Taken from [14, 15].

used. Moreover the microcavity consists of two highly reflective, spherical mirrors, which trap the electrical field inside the resonator and also introduce a harmonic trapping potential (see Fig.1.2(a)). Due to the interaction of the photons with the dye-molecules an effective photon-photon interaction is generated.
Furthermore the cavity as the second important step allows the introduction of a quadratic dispersion relation and a cutoff frequence as shown in Fig.1.2(b)). This provides a ground state for the photons. In addition, the photon gas behaves like a massive Bose gas due to the quadratic dispersion, which means that a mass analogue can be introduced [13].
Moreover due to imperfections of the mirrors photons can also leave the cavity and thus yields a loss rate, which can be directly measured.
With this mechanism it is possible to tune the photon number above a critical threshold, as shown in Fig.1.2 (c,d)

1.2.2. Theoretical Foundations

To describe a PBEC theoretically on a mean-field level necessitates a description of both the temperature diffusion through the dye-solution and the photon BEC. As described in [13] one can model the diffusion through the dye-solution by introducing a diffusion equation and the photon BEC by its mean-field wave function fulfilling the wave equation in the cavity. This model is also formally analogous to models of incoherent pumped polariton-exciton condensates [13, 16].
However in this thesis we consider a different theoretical approach. We know that a BEC without pumping and losses of particles can be described by the Gross-Pitaevskii equation (GPE) first introduced in 1961 by Pitaevskii [17] and Gross [18]. This equation is formally a nonlinear, time-dependent Schrödinger equation. Due to stimulated emission, it can be derived in a phenomenological way in the case of a PBEC, that an additional imaginary nonlinear term is obtained in the GPE taking into account the laser rate equations for a two-level model [19].

1.3. Vortices in Quantum Gases

In classical hydrodynamics, vortices refer to swirling patterns or regions within a fluid where the flow revolves around an axis line. They are often observed in liquids or gases and are characterized by a rotating motion. Natural occurrences of vortices are seen in phenomena such as tornadoes in the atmosphere and whirlpools in bodies of water. These large-scale vortices can have significant effects on their surroundings due to their energy and rotational movement [20].
In the first part of this section we discuss vortices in closed systems, so without any particle gains and losses, and secondly we then proceed to open dissipative systems like a PBEC and discuss how the open dissipative property effects vortices.

1.3.1. Vortices in Closed Systems

Vortices in quantum mechanics represent fascinating phenomena where particles or fields exhibit intricate rotational motion within a quantum setting. These vortices emerge across diverse domains, from superfluids and superconductors to quantum gases. In quantum fluids like superfluid helium or Bose-Einstein condensates, vortices appear as topological defects in the fluid's flow [21]. These vortex structures play a crucial role in understanding the dynamics and properties of several quantum systems.
However the most important difference of quantum vortices and those in classical hydrodynamics is the quantized circulation due to the singled-valuedness of the condensate wave function.
The first realization of quatum vortices was achieved in 1999 [22]. Quantum vortices in BECs can be created using different techniques. One common method involves stirring the BEC using laser beams or magnetic fields, creating a rotating potential

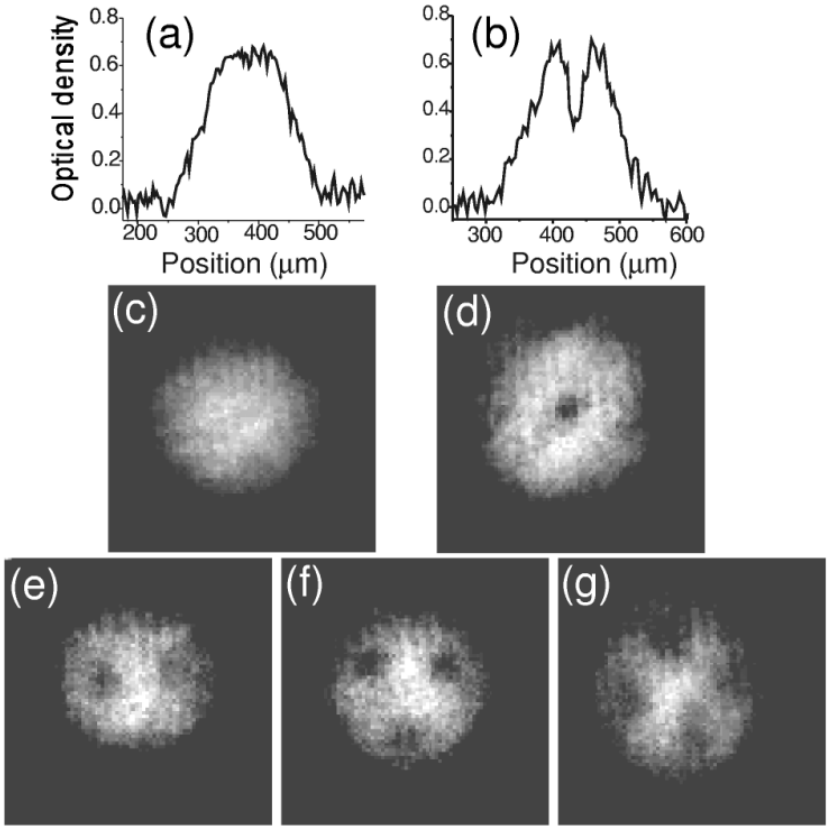

Figure 1.3.: Absorption images of a stirred Bose-Einstein condensate. (a) and (b) show the optical thickness of the cloud along the horizontal axis. (c)-(g) show the appearance of zero up to four vortices. Taken from [23].

that induces the formation of vortices [23] (see Fig.1.3).

1.3.2. Vortices in Open Dissipative Systems

Photon condensates are in good approximation an ideal Bose gas, which limits its possibilities to study vortices, because the core size becomes as large as the entire system [5]. This is related to the infinite compressibility of an ideal Bose gas, which leads to large density fluctuations. Therefore it is prevented to have a well defined phase degree of freedom. But due to the presence of losses in a PBEC and therefore a compensating pumping, PBEC differs from an ideal Bose gas. So due to the interplay of losses and pumping density fluctuations can be reduced and form a well defined photon phase.
Considering an array of photon condensates [24], which are coupled by tunneling,

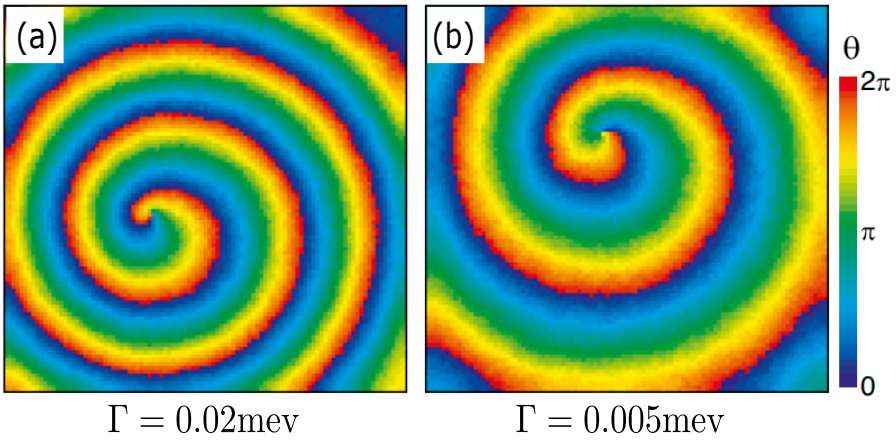

Figure 1.4.: Phase of the wave function for different values of losses Γ. Taken from [24].

one can model the system by a generalized Gross-Pitaevski equation

$$i\hbar\frac{\partial\psi(\mathbf{x},t)}{\partial t} = -(1-i\kappa)J\sum_{\mathbf{x}'\in\mathcal{N}_\mathbf{x}} + V(\mathbf{x})\psi(\mathbf{x}) + \frac{i}{2}\left[B_{21}M_2(\mathbf{x}) - B_{12}M_1(\mathbf{x}) - \Gamma\right]\psi(\mathbf{x})\,, \tag{1.1}$$

where J denotes the coupling strength, V an external potential, γ the loss rate of the system and B_{12}, B_{21} the Einstein coefficients for emission and absortion. Furthermore we note that in equation (1.1) there is no explicit interaction term known from the GPE, but instead it is claimed that the κ-term acts like an interaction term. With this one can then investigate numerically the emergence of vortices. Considering one single vortex a numerical simulation shows that the phase of the wave function has a spiral shape (see Fig.1.4). Also we see because the phase is directly related to the velocity field that also the velocity field has a spiral shape. Due to the continuous pumping of photons we therefore note that the direction of the corresponding flow points outwards the system, to avoid a divergence of density. Therefore one can see that a single vortex in a PBEC acts like a particle source.

1.4. Outline

In this thesis we work out an analytical solution for a photon condensate in presence of a single vortex. To this end the thesis consists of three parts. The first part is dedicated to give an introduction into the used model and how to describe the system with hydrodynamic equations. In Chapter 2 we introduce the used complex Gross-Pitaevskii equation. Therefore we start with the derivation of the standard GPE, which is used to describe atomic BECs. Afterwards we derive on a phenomenological level the complex GPE describing also pumping and losses. In Chapter 3 we introduce the hydrodynamic description of a Bose-Einstein condensate in a closed system by applying the Madelung transformation to the GPE and then discussing the changes in the hydrodynamic equations for the open dissipative system.

In the second part, we introduce in Chapter 4 analytical methods for approximately solving the underlying equations of motion described from a mathematical point of view. This part is splitted it three sections. First we starting by introducing shortly the least action priciple, which based on minimizing the corresponding action. Afterwards due the lack of energy conservation in open systems we introduce as a first method for open dissipative systems the cumulant optimization method, which is only valid for exponential like wave functions. To overcome this issue of the cumulant optimization method we then construct in the last section of this part a new method [25] for solving all kinds of equations of motion, which is independent of the underlying wave function.

In the last part, which consists of three chapters we consider at first in Chapter 5 an open dissipative system in presence of an external harmonic potential and calculate an approximate solution using both the cumulant and the projection optimization method [25] for different ansatz wave functions. We also compare the results from the cumulant and projection optimization method and show explicitly that both methods are equivalent. Afterwards in Chapter 6 we use the projection optimization method for an homogeneous system in presence of a single vortex. This will lead to an approximate solution of the density and the velocity field and we will see that also in the analytical solution we get a spiral shaped velocity field. The comparison of all results together with the numerical simulations then leads to a good match. In Chapter 7 we consider the continuum model of (1.1) and show that the imaginary κ-term behaves, indeed, as an interaction term.

2. Mean-Field Model of Interacting Bose Gas in BEC Phase

The description of an ideal Bose gas is based on methods of statistical mechanics, in which the gas can be described as a union of independent atoms due to the lack of particle-particle interaction [26]. However, these techniques do not work for an interacting Bose gas.
In this chapter we will derive the Gross-Pitaevskii equation (GPE), which describes the evolution of the order parameter of an interacting BEC. Afterwards, we generalize the GPE to interacting Bose gases for open dissipative systems by adding heuristically an additional term to the GPE due to particle gain and loss. However, note this can also be derived by an gradient expansion of a path-integral theory [27] or considering a Lindblad master equation [28].

2.1. The Gross-Pitaevskii Equation

In this section we derive the equation of motion for an interacting Bose gas in the BEC phase. From Penrose and Onasger [29] we know that the essential quantity of describing a Bose gas of N interacting particles is given by the order parameter $\psi(\mathbf{r})$. This order parameter is defined with the eigenvector Θ_0 of the reduced density matrix $\rho(\mathbf{r}, \mathbf{r}')$, which is related to the many-body wave function $\Psi(\mathbf{r}_1, ..., \mathbf{r}_N)$ of the system

$$\rho(\mathbf{r}, \mathbf{r}') = N \int d\mathbf{r}_2 ... d\mathbf{r}_N \Psi^*(\mathbf{r}, ..., \mathbf{r}_N)\Psi(\mathbf{r}', ..., \mathbf{r}_N) \tag{2.1}$$

as

$$\psi(\mathbf{r}) = \sqrt{N_0}\Theta_0(\mathbf{r})\,. \tag{2.2}$$

In (2.2) N_0 corresponds to the largest eigenvalue of (2.1), which is also interpreted as the condensed particles in the BEC phase. Note that the eigenvector Θ_0 of (2.1) does exist due to the hermiticity of the density matrix according to the spectral theorem [30].

As the order parameter describes the global behaviour of the system it is also referred to be the condensate wave function [31]. Furthermore by definition the order parameter has the properties

$$\int d\mathbf{r}\, |\psi(\mathbf{r})|^2 = N_0 \tag{2.3}$$

$$|\psi(\mathbf{r})|^2 = \rho(\mathbf{r}, \mathbf{r})\,, \tag{2.4}$$

where the latter (2.4) represents the condensate density.
To derive the equation of motion for the condensate wave function we consider the Hamiltonian of the system in second quantization:

$$\hat{H} = \int d\mathbf{r}\, \hat{\psi}^\dagger(\mathbf{r}) \left\{ -\frac{\hbar^2}{2m}\boldsymbol{\nabla}^2 + V(\mathbf{r}) \right\} \hat{\psi}(\mathbf{r}) + \frac{1}{2}\int d\mathbf{r} \int d\mathbf{r}'\, \hat{\psi}^\dagger(\mathbf{r})\hat{\psi}^\dagger(\mathbf{r}')U(\mathbf{r}-\mathbf{r}')\hat{\psi}(\mathbf{r}')\hat{\psi}(\mathbf{r})\,, \tag{2.5}$$

which was first introduced in 1961 by E.P. Gross [18] and L.P. Pitaevskii [17]. In Eq. (2.5) the first term in the integrand denotes the kinetic term, V an external potential and U the particle-particle interaction.
With using the commutation relations for bosons [32]

$$\left[\hat{\psi}(\mathbf{r},t), \hat{\psi}^\dagger(\mathbf{r}',t)\right]_- = \delta(\mathbf{r}-\mathbf{r}')\,,\ \left[\hat{\psi}(\mathbf{r},t), \hat{\psi}(\mathbf{r}',t)\right]_- = 0 = \left[\hat{\psi}^\dagger(\mathbf{r},t), \hat{\psi}^\dagger(\mathbf{r}',t)\right]_- \tag{2.6}$$

the Heisenberg equation of motion for the field operator $\hat{\psi}(\mathbf{r},t)$ can be calculated

$$i\hbar\frac{\partial\hat{\psi}(\mathbf{r},t)}{\partial t} = \left[\hat{\psi}(\mathbf{r},t), \hat{H}\right]_- . \tag{2.7}$$

Making now Bogoliubov's assumption [33] that the BEC state is given by the order parameter

$$\hat{\psi}(\mathbf{r},t) \approx \psi(\mathbf{r},t) \tag{2.8}$$

and assuming a short-range particle-particle interaction via $U(\mathbf{r}-\mathbf{r}') = \delta(\mathbf{r}-\mathbf{r}')$ yields the time dependent Gross-Pitaevskii equation

$$i\hbar\frac{\partial\psi(\mathbf{r},t)}{\partial t} = \left\{ -\frac{\hbar^2}{2m}\boldsymbol{\nabla}^2 + V(\mathbf{r}) + g\left|\psi(\mathbf{r},t)\right|^2 \right\} \psi(\mathbf{r},t)\,, \tag{2.9}$$

where the interaction strength g is given by

$$g = \int d\mathbf{r}\, U(\mathbf{r})\,. \tag{2.10}$$

Note that the GPE (2.9) can be interpreted as a non-linear Schrödinger equation, where the nonlinearity is created by the particle-particle interaction.
For seperating spatial and time contribution of the wave function perform the ansatz

$$\psi(\mathbf{r},t) = \psi(\mathbf{r})e^{-\frac{i}{\hbar}\mu t}\,, \tag{2.11}$$

where μ denotes the chemical potential and is determined by the normalization condition (2.3). Inserting the ansatz (2.11) into the time-dependent GPE (2.9) results in the time independent GPE

$$\mu\psi(\mathbf{r}) = \left\{ -\frac{\hbar^2}{2m}\boldsymbol{\nabla}^2 + V\left(\mathbf{r}\right) + g\left|\psi(\mathbf{r})\right|^2 \right\} \psi(\mathbf{r})\,, \tag{2.12}$$

which describes stationary states of the condensate.

2.2. The Complex Gross-Pitaevskii Equation

For the theoretical description of the dynamics of a Bose-Einstein condensate in an open dissipative system one has to extend the GPE (2.9) and also include terms appearing due to particle pumping and decay [34].

2.2.1. Heuristical Derivation

As the GPE only describes condensates, where the particles are caught in the system we therefore have to include additional terms for open dissipative condensates like a PBEC. So we have to find these terms describing also the effect of particle pumping and losses as this leads to an increase or decrease of the condensate density. This yields then a generalized GPE called the complex Gross-Pitaevskii equation (cGPE). Considering nonresonant pumping and also introducing stimulated scattering yields an equation for particle gains [34]

$$\hbar\frac{\partial\psi(\mathbf{r},t)}{\partial t} = \gamma\psi\,, \tag{2.13}$$

where γ denotes the rate of particle gain. Furthermore introducing a constant global loss rate leads to

$$\hbar\frac{\partial\psi(\mathbf{r},t)}{\partial t} = -\kappa\psi\,, \tag{2.14}$$

where κ represents the rate of particle losses. Combining Eq. (2.13) and Eq. (2.14) yields an effective open system parameter

$$\lambda = \gamma - \kappa\,. \tag{2.15}$$

However, with such a modeling he dynamics becomes unstable as numerical simulations reveal. If gains exceeds losses, according to Eq. (2.15) λ is positive and thus leads to an infinite increase in the condensate density. And conversely, if losses are higher than gains, this leads to a negative λ and thus to a vanishing condensate. Because of that and knowing that in reality the condensate density can be brought to a stationary state, it is necessary to use a different model.
The simplest model is given by a density dependent loss term

$$\hbar\frac{\partial\psi(\mathbf{r},t)}{\partial t} = \left(\gamma - \Gamma\left|\psi(\mathbf{r},t)\right|^2\right)\psi(\mathbf{r},t)\,, \tag{2.16}$$

where γ stands for the pumping rate and Γ denotes the losses. Indeed for a Photon BEC a density dependent loss rate is needed to also describe the dye bleaching [12, 15], which is a limiting factor of a single experimental cycle.
Note this kind of model is also used in exciton-polariton condensates [16].
This leads to the following equation of motion

$$i\hbar\frac{\partial\psi(\mathbf{r},t)}{\partial t} = \left\{-\frac{\hbar^2}{2m}\boldsymbol{\nabla}^2 + V(\mathbf{r}) + g\left|\psi(\mathbf{r},t)\right|^2 + \frac{i}{2}\left[\gamma - \Gamma\left|\psi(\mathbf{r},t)\right|^2\right]\right\}\psi(\mathbf{r},t)\,, \tag{2.17}$$

which describes an open dissipative condensate.
Furthermore analogue to the closed system case we also can separate the time dependence of the wave function with the ansatz (2.11) yielding the cGPE describing a steady-state

$$\mu\psi(\mathbf{r}) = \left\{ -\frac{\hbar^2}{2m}\boldsymbol{\nabla}^2 + V(\mathbf{r}) + g\left|\psi(\mathbf{r})\right|^2 + \frac{i}{2}\left[\gamma - \Gamma\left|\psi(\mathbf{r})\right|^2\right] \right\} \psi(\mathbf{r})\,. \tag{2.18}$$

2.2.2. Linear Stability Analysis

To have better insight into the mean-field model (2.17) we start with analysing the homogeneous case, i.e. $V = 0$

$$i\hbar\frac{\partial\psi(\mathbf{r},t)}{\partial t} = \left\{ -\frac{\hbar^2}{2m}\boldsymbol{\nabla}^2 + g\left|\psi(\mathbf{r},t)\right|^2 + \frac{i}{2}\left[\gamma - \Gamma\left|\psi(\mathbf{r},t)\right|^2\right] \right\} \psi(\mathbf{r},t)\,. \tag{2.19}$$

Note that we are considering a BEC without a trapping potential in two dimensions, which does not exist according to the Mermin-Wagner-Hohenberg theorem [35–37]. However, this theorem is only valid for closed systems and therefore can not be applied to our case.
Now we start our calculation by linearizing the cGPE (2.19). For this purpose we make the ansatz [16]

$$\psi(\mathbf{r},t) = \psi_0(\mathbf{r},t) + \delta\psi(\mathbf{r},t)\,, \tag{2.20}$$

where the steady state solution of (2.19) represents the zeroth order

$$\psi_0(\mathbf{r},t) = \sqrt{n_0}e^{-\frac{i}{\hbar}\mu t} \tag{2.21}$$

with the equilibrium density n_0 and the chemical potential μ.. Calculating the large distance behavior of the stationary cGPE (2.18) in a homogeneous system without a trap we get relations for the chemical potential μ as well as for the steady state density n_0

$$\mu = gn_0\,,\; n_0 = \frac{\gamma}{\Gamma} \tag{2.22}$$

connecting these parameters with the pumping γ and losses Γ.
Furthermore $\delta\psi$ stands for a small perturbation from the stationary state. Inserting the ansatz (2.20) into the cGPE (2.19) and neglecting all higher orders of $\delta\psi$ starting with $\delta\psi^2$ yield

$$\begin{aligned} i\hbar\frac{\partial\delta\psi}{\partial t} = -\frac{\hbar^2}{2m}\boldsymbol{\nabla}^2\delta\psi + g\left[2\left|\psi_0\right|^2\delta\psi + \psi_0^2\delta\psi^*\right] \\ + \frac{i}{2}\left[\gamma\delta\psi - \Gamma\left(2\left|\psi_0\right|^2\delta\psi + \psi_0^2\delta\psi^*\right)\right] \end{aligned} \tag{2.23}$$

and also for the complex conjugated cGPE (2.19) we get

$$\begin{aligned} -i\hbar\frac{\partial\delta\psi^*}{\partial t} = -\frac{\hbar^2}{2m}\boldsymbol{\nabla}^2\delta\psi^* + g\left[2\left|\psi_0\right|^2\delta\psi^* + \left(\psi_0^*\right)^2\delta\psi\right] \\ - \frac{i}{2}\left[\gamma\delta\psi^* - \Gamma\left(2\left|\psi_0\right|^2\delta\psi^* + \left(\psi_0^*\right)^2\delta\psi\right)\right]\,. \end{aligned} \tag{2.24}$$

To find solutions of (2.23) and (2.24) we make the following Fourier ansatz for the perturbation $\delta\psi$ [13, 16, 38]

$$\delta\psi(\mathbf{r},t) = e^{-\frac{i}{\hbar}\mu t}\left[u(\mathbf{r})e^{-i\omega t} - v^*(\mathbf{r})e^{i\omega^* t}\right] \tag{2.25}$$

where u, v are yet unknown functions and ω is complex. Note that the minus sign in (2.25) is just a matter of convention [38]. Furthermore to ensure a stable steady state we have to include a damping term, which leads to a complex valued ω and therefore to a stable stationary state iff $\mathrm{Im}(\omega) < 0$. Note that this is a major contrast to a corresponding calculation for the GPE (2.9) in closed systems, where ω is a purely real quantity [38].
Inserting the ansatz (2.25) and the steady state solution (2.21) into (2.23) results in

$$\begin{aligned}
&\mu\left[ue^{-i\omega t} - v^*e^{i\omega^* t}\right] + \hbar\omega ue^{-i\omega t} - \hbar\omega^* v^* e^{i\omega^* t} = -\frac{\hbar^2}{2m}\left[\boldsymbol{\nabla}^2 ue^{-i\omega t} - \boldsymbol{\nabla}^2 v^* e^{i\omega^* t}\right] \\
&+ g\left[2n_0 ue^{-i\omega t} - 2n_0 v^* e^{i\omega^* t} + n_0 u^* e^{i\omega^* t} - n_0 ve^{-i\omega t}\right] \\
&+ \frac{i}{2}\left[\gamma ue^{-i\omega t} - \gamma v^* e^{i\omega^* t} - 2\Gamma n_0 ue^{-i\omega t} + 2\Gamma n_0 v^* e^{i\omega^* t} - \Gamma n_0 u^* e^{i\omega^* t} + \Gamma n_0 ve^{-i\omega t}\right]
\end{aligned} \tag{2.26}$$

Comparing coefficients of $e^{-i\omega t}$ and $e^{i\omega^* t}$ leads to the Bogoliubov equations

$$\left[-\frac{\hbar^2}{2m}\boldsymbol{\nabla}^2 + 2gn_0 - \mu - \hbar\omega + \frac{i}{2}(\gamma - 2\Gamma n_0)\right]u + \left[-gn_0 + \frac{i}{2}\Gamma n_0\right]v = 0 \tag{2.27}$$

$$\left[-\frac{\hbar^2}{2m}\boldsymbol{\nabla}^2 + 2gn_0 - \mu - \hbar\omega - \frac{i}{2}(\gamma - 2\Gamma n_0)\right]v - \left[gn_0 + \frac{i}{2}\Gamma n_0\right]u = 0\,, \tag{2.28}$$

where the latter equation (2.28) was complex conjugated. Note that it is equivalent to insert the ansatz (2.25) and the steady state solution (2.21) into (2.24).
Due to translational invariance we make the following ansatzes

$$u(\mathbf{r}) = u_k e^{i\mathbf{k}\cdot\mathbf{r}} \tag{2.29}$$

$$v(\mathbf{r}) = v_k e^{i\mathbf{k}\cdot\mathbf{r}}\,. \tag{2.30}$$

Inserting the ansatzes (2.29) and (2.30) into (2.27) and (2.28) leads to a system of linear equations

$$\begin{pmatrix} E_0 + 2gn_0 - \mu - \hbar\omega + \frac{i}{2}(\gamma - 2\Gamma n_0) & \frac{i}{2}\Gamma n_0 - gn_0 \\ -\left(\frac{i}{2}\Gamma n_0 + gn_0\right) & E_0 + 2gn_0 - \mu + \hbar\omega - \frac{i}{2}(\gamma - 2\Gamma n_0) \end{pmatrix}\begin{pmatrix} u_k \\ v_k \end{pmatrix} = 0\,, \tag{2.31}$$

where the free particle dispersion was introduced [38]

$$E_0 = \frac{\hbar^2 k^2}{2m}\,. \tag{2.32}$$

To simplify the notation we denote in the following the matrix in (2.31) as A. In order for the equation (2.31) to have a consistent solution, we require that the determinant

of the matrix A vanishes. Therefore calculating the characteristic polynomial of the matrix A gives us

$$p_A(\omega) = (\hbar\omega)^2 - i\left(\gamma - 2\Gamma n_0\right)\hbar\omega - (E_0 + 2gn_0 - \mu)^2 - \left(\frac{\gamma - 2\Gamma n_0}{2}\right)^2 + \left(\frac{\Gamma n_0}{2}\right)^2 + (gn_0)^2 \tag{2.33}$$

Using the relations (2.22) in (2.33) yields

$$p_A(\omega) = (\hbar\omega)^2 - i\gamma\hbar\omega + (E_0 + gn_0)^2 + (gn_0)^2 \,. \tag{2.34}$$

Calculating all zeros of the characteristic polynomial (2.34) and therefore the eigenvalues for the matrix A in (2.31) we get

$$E(\mathbf{k}) = -i\frac{\gamma}{2} \pm \sqrt{E_0\left(E_0 + 2gn_0\right) - \frac{\gamma^2}{4}} \,. \tag{2.35}$$

Therefore we directly see that in the closed system limit $\gamma \to 0$ the dispersion relation reduces to the standard Bogoliubov dispersion [38]. First note that both eigenmodes are stable due to a negative imaginary part.
The upper + branch in (2.35) is the Goldstone branch [16], because this converges in the limit $\mathbf{k} \to 0$. Expanding the upper branch in (2.35) for small $\mathbf{k}$-vectors

$$E(\mathbf{k}) \approx -i\frac{\gamma}{2} + i\frac{\gamma}{2}\left(1 - \frac{2gn_0}{\gamma^2}E_0\right) = 0 + \mathcal{O}(k^2) \tag{2.36}$$

we directly note the appearance of the Goldstone theorem [39], which is also shown in Fig.2.2 . Secondly the lower branch, where its long wave vector behavior corresponds to a damped free particle

$$E(\mathbf{k}) = -i\frac{\gamma}{2} - E_0 \,, \tag{2.37}$$

but an expansion for short wave vectors yields

$$E(\mathbf{k}) = -i\gamma + \mathcal{O}(E_0^2) \tag{2.38}$$

Therefore the real part of the lower branch violates the Goldstone theorem and yields a flat region of the Goldstone mode in k-space, see Fig. 2.1. This also can be quantified by calculating the zeros of the square root argument and results in

$$E_0^2 + \frac{2g\gamma}{\Gamma}E_0 - \frac{\gamma^2}{4} = 0 \;\Rightarrow\; \tilde{E}_0 = \left(-\frac{g}{\Gamma} \pm \sqrt{\left(\frac{g}{\Gamma}\right)^2 + \frac{1}{4}}\right)\gamma \,. \tag{2.39}$$

Note that in (2.39) only the +-solution is physically relevant, because otherwise a negative energy dependent on the interaction strength and losses occur.

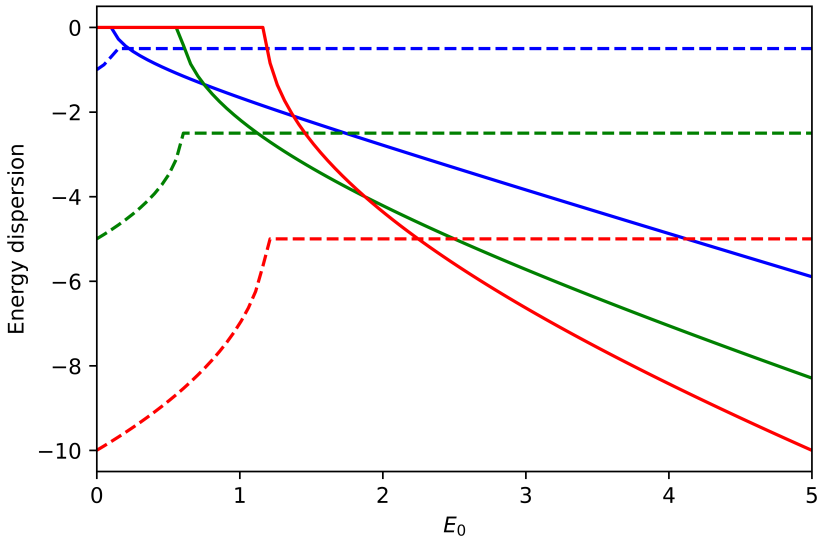

Figure 2.1.: Real part (solid lines) and imaginary part (dotted lines) of the lower branch of the energy dispersion (2.35). Plottet for fixed $g/\Gamma = 1$ and $\gamma = 1$ (red color), $\gamma = 5$ (green color), $\gamma = 10$ (blue color).

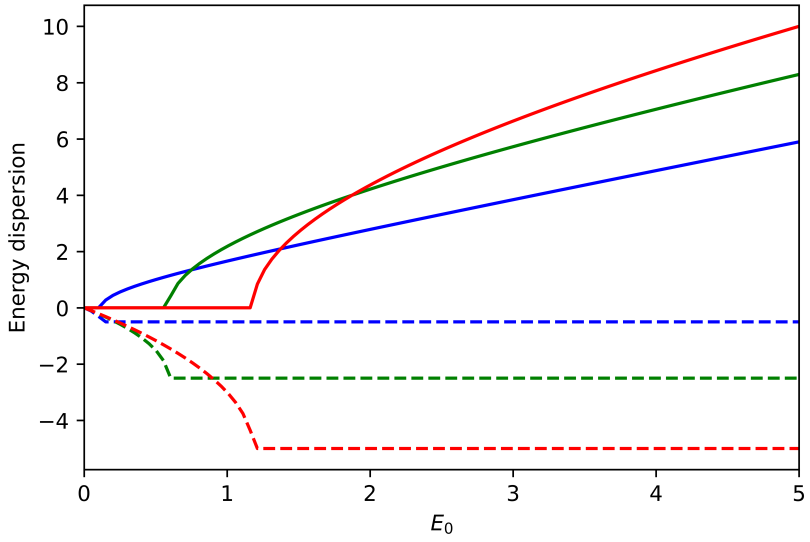

Figure 2.2.: Real part (solid lines) and imaginary part (dotted lines) of the upper branch of the energy dispersion (2.35). Plottet for fixed $g/\Gamma = 1$ and $\gamma = 1$ (red color), $\gamma = 5$ (green color), $\gamma = 10$ (blue color).

3. Hydrodynamic Description

An alternative description of the BEC phase using the condensate density and velocity is derived in this chapter. We first derive the hydrodynamic equations in the case of a closed system, which can be described according to the first Chapter with the GPE. Afterwards we focus on the open dissipative case and derive the hydrodynamic equations.

3.1. Closed System

Multiplication of the GPE (2.9) with ψ^* and vice versa the complex conjugated GPE with ψ yields after substracting

$$\frac{\partial |\psi|^2}{\partial t} + \boldsymbol{\nabla} \cdot \left\{ \frac{\hbar}{2mi} \left[\psi^* \boldsymbol{\nabla} \psi - \psi \boldsymbol{\nabla} \psi^* \right] \right\} = 0 \,. \tag{3.1}$$

We note that (3.1) coincides the continuity equation for the Schrödinger field, which is an equation for the probability density [38]. Therefore by identifying the expression in brackets as a current field, i.e. a velocity field times the density, we get for the velocity field the expression

$$\mathbf{v} = \frac{\hbar}{2mi} \frac{\psi^* \boldsymbol{\nabla} \psi - \psi \boldsymbol{\nabla} \psi^*}{\psi^* \psi} \,. \tag{3.2}$$

With this the continuity equation can be written in the compact form

$$\frac{\partial n}{\partial t} + \boldsymbol{\nabla}(n\mathbf{v}) = 0 \,, \tag{3.3}$$

where $n = |\psi|^2$ denotes the condensate density and $n\mathbf{v} := \mathbf{j}$ can be identified as the current density.
Furthermore using the Madelung representation by writing the order parameter as

$$\psi(\mathbf{r}, t) = \sqrt{n(\mathbf{r}, t)} e^{i\Phi(\mathbf{r}, t)} \tag{3.4}$$

one calculates for the velocity

$$\mathbf{v}(\mathbf{r}, t) = \frac{\hbar}{m} \boldsymbol{\nabla} \Phi(\mathbf{r}, t) \,. \tag{3.5}$$

Therefore the phase of the wave function is directly related to the condensate velocity.

3.1.1. Hydrodynamic Equations in 3D

Since the density and the velocity contain according to (3.4) the same information as the condensate wave function we now derive the respective equations of motion. Inserting the Madelung representation (3.4) in the GPE (2.9), we get

$$\begin{aligned} & i\hbar\left[\frac{1}{2\sqrt{n}}\frac{\partial n}{\partial t}+i\sqrt{n}\frac{\partial\Phi}{\partial t}\right]e^{i\Phi}= \\ =&-\frac{\hbar^2}{2m}\left[\frac{\boldsymbol{\nabla}^2 n}{2\sqrt{n}}-\frac{(\boldsymbol{\nabla}n)^2}{4\sqrt{n}^3}+i\frac{\boldsymbol{\nabla}n\boldsymbol{\nabla}\Phi}{\sqrt{n}}+i\sqrt{n}\boldsymbol{\nabla}^2\Phi-\sqrt{n}\left(\boldsymbol{\nabla}\Phi\right)^2\right]e^{i\Phi} \\ &+V\sqrt{n}e^{i\Phi}+g\sqrt{n}^3e^{i\Phi}\,. \end{aligned} \tag{3.6}$$

Separating real and imaginary part of (3.6) yields

$$\frac{\partial\varphi}{\partial t}=\frac{\hbar}{4m}\left[\frac{\boldsymbol{\nabla}^2 n}{n}-\frac{(\boldsymbol{\nabla}n)^2}{2n^2}-2\left(\boldsymbol{\nabla}\varphi\right)^2\right]-\frac{V}{\hbar}-\frac{gn}{\hbar}\,, \tag{3.7}$$

$$\frac{\partial n}{\partial t}=-\frac{\hbar}{m}\left[\boldsymbol{\nabla}n\boldsymbol{\nabla}\varphi+n\boldsymbol{\nabla}^2\varphi\right]\,. \tag{3.8}$$

Taking the gradient of (3.7) and inserting the identity

$$\frac{\boldsymbol{\nabla}^2 n}{n}-\frac{(\boldsymbol{\nabla}n)^2}{2n^2}=2\frac{\boldsymbol{\nabla}^2\sqrt{n}}{\sqrt{n}} \tag{3.9}$$

into (3.7) and, furthermore, using the expression of the velocity field (3.5) results in the hydrodynamic equations

$$\frac{\partial n}{\partial t}+\boldsymbol{\nabla}\left(n\cdot\mathbf{v}\right)=0\,, \tag{3.10}$$

$$\frac{\partial\mathbf{v}}{\partial t}-\boldsymbol{\nabla}\left\{\frac{\hbar^2}{2m^2}\frac{\boldsymbol{\nabla}^2\sqrt{n}}{\sqrt{n}}-\frac{1}{2}\mathbf{v}^2-\frac{V}{m}-\frac{gn}{m}\right\}=0\,. \tag{3.11}$$

The first equation (3.10) corresponds to the continuity equation for the particle density (3.3), whereas the second equation (3.11) denotes a Newton equation. This second equation (3.11) can be rewritten using the vector identity

$$\frac{1}{2}\boldsymbol{\nabla}\mathbf{v}^2=\left(v\cdot\boldsymbol{\nabla}\right)v-\left(\boldsymbol{\nabla}\times\mathbf{v}\right)\times\mathbf{v}\,. \tag{3.12}$$

This leads to the Euler or quantum Bernoulli equation

$$\frac{\partial\mathbf{v}}{\partial t}+\left(v\cdot\boldsymbol{\nabla}\right)v=-\boldsymbol{\nabla}\left[\frac{V}{m}+\frac{gn}{m}-\frac{\hbar^2}{2m^2}\frac{\boldsymbol{\nabla}^2\sqrt{n}}{\sqrt{n}}\right]+\left(\boldsymbol{\nabla}\times\mathbf{v}\right)\times\mathbf{v}\,. \tag{3.13}$$

Concluding, because the condensate velocity fulfills the Euler equation with an additional vorticity term, that the condensate behaves like a flow without friction [31]. Note that the left-hand side of (3.13) represents a material derivative and therefore

denotes the time derivative of an observer flowing with the current. Additionally we discuss each term in the Euler equation (3.13). Note that the first term on the right-hand side of (3.13) represents a pressure, which contains three terms. The first pressure term is the mechanical pressure introduced by an external trapping potential. The second term is the interaction pressure due to repulsive interactions between the atoms. The third and last pressure is the quantum pressure, which shows the resistance against deformation of the wave function. The last term on the right hand side of (3.13) acts like a Lorenzian force and appears only if the velocity field has a singularity.
Therefore in presence of vortices we have also have to take into account that turbulences appear in the velocity field. We define therefore over the curl of the velocity field the vorticity

$$\boldsymbol{\omega}(\mathbf{r},t) = \boldsymbol{\nabla} \times \mathbf{v}(\mathbf{r},t)\,, \tag{3.14}$$

which is in principle a measure on how turbulent the system is. With that definition we can now derive a third hydrodynamic equation for the vorticity (3.14). By taking the curl of the Euler equation (3.13) we derive the Helmholtz vorticity equation

$$\frac{\partial \boldsymbol{\omega}}{\partial t} + (\mathbf{v}\cdot\boldsymbol{\nabla})\,\boldsymbol{\omega} = (\boldsymbol{\omega}\cdot\boldsymbol{\nabla})\,\mathbf{v} - \boldsymbol{\omega}\cdot(\boldsymbol{\nabla}\cdot\mathbf{v})\,. \tag{3.15}$$

Note that the latter is also well known in classical hydrodynamics. For further interest we refer to [40].

3.1.2. Hydrodynamic Equations in 2D

Of special interest for this thesis is a description of a two-dimensional condensate in presence of singularities in the condensate phase. Therefore we work out a description of a system involving also vortices in two dimensions.
Knowing from (3.5) that the condensate velocity field is directly proportional to the gradient of the phase we conclude in the absence of singularities for the phase

$$\boldsymbol{\omega} = \boldsymbol{\nabla} \times \mathbf{v} = \frac{\partial^2\Phi}{\partial x \partial y} - \frac{\partial^2\Phi}{\partial y \partial x} = 0\,. \tag{3.16}$$

But in presence of a vortex, where we assume its location without loss of generality at the origina, the phase has a singularity at $x = y = 0$ and therefore we get

$$\boldsymbol{\omega} = \boldsymbol{\nabla} \times \mathbf{v} = \frac{\partial^2\Phi}{\partial x \partial y} - \frac{\partial^2\Phi}{\partial y \partial x} \neq 0\,. \tag{3.17}$$

Note that the latter statement (3.17) is equivalent to the fact that the phase is not twice continuously differentiable and thus Schwarz's theorem does not hold [41]. Due to the single-valuedness of the condensate wave function we get, by integrating around a closed contour, that the change in the phase Φ in two dimensions must be a multiple of 2π. Thus the circulation Z, which is defined as

$$Z = \oint \mathbf{v}\cdot d\mathbf{r} \tag{3.18}$$

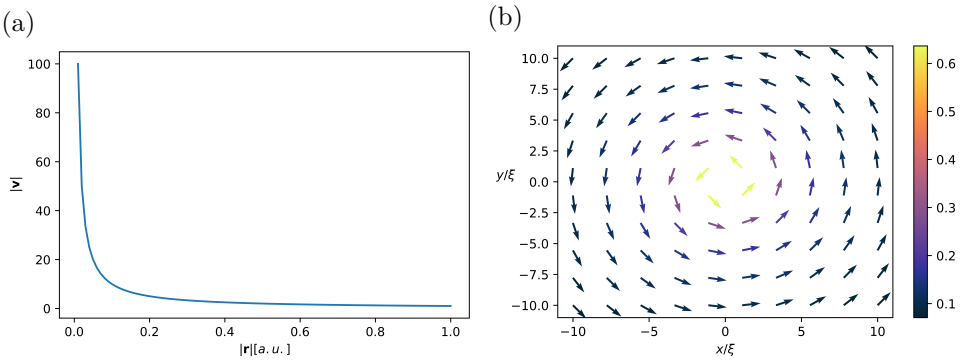

Figure 3.1.: (a) Tangential velocity field of single vortex in arbitrary units diverges at the origin. (b) velocity field in two dimensions. The color of the arrows shows the strength of the velocity field.

results, by using (3.5) and Stoke's theorem, in

$$Z = 2\pi \frac{\hbar}{m} l \,, \tag{3.19}$$

where l is an integer and represents the winding number of the flow. The winding number is often also referred in case of a vortex as the charge of the vortex. Note that the quantization of the circulation was first proposed by Onsager [42] in 1949 for superfluid helium and by Feynman in 1955 [43].
As an example we now consider a purely azimuthal flow, which represents a vortex line straight in z-direction [38]. Therefore we consider a phase

$$\Phi = \arctan\left(\frac{y}{x}\right) \tag{3.20}$$

with the corresponding velocity field according to (3.5)

$$\mathbf{v}(\mathbf{r}) = \frac{\hbar}{m} \boldsymbol{\nabla} \varphi(\mathbf{r}) = \frac{\hbar}{m} \frac{1}{r} \mathbf{e}_{\varphi} \,, \tag{3.21}$$

where $r = |\mathbf{r}|$ denotes the radial distance and $\mathbf{e}_{\varphi}$ the unit vector in polar coordinates. Therefore we see that the velocity field is singular at the origin, which is also plotted in Fig. 3.1. We know from (3.20) that the phase has a singularity at the origin and is directly related to the velocity field (3.5). So the velocity field is represented by a non continuous function. To overcome this and write the velocity field with a continuous function for which also the theorem of Schwarz is valid we consider instead a different approach. To this end we define a function, which is called the stream function χ, in the following sense [44, 45]

$$\mathbf{v}(\mathbf{r}) = \frac{\hbar}{m} \begin{pmatrix} -\frac{\partial \chi(\mathbf{r})}{\partial y} \\ \frac{\partial \chi(\mathbf{r})}{\partial x} \end{pmatrix} . \tag{3.22}$$

This has the advantage that the continuity equation in the far field, where the density is nearly constant, reads

$$\boldsymbol{\nabla} \cdot \mathbf{v} = 0\,, \tag{3.23}$$

so the stream function is twice continuously differentiable and the theorem of Schwarz can be applied. To derive the stream function for a single vortex at the origin we consider the vorticity from (3.14) and (3.22)

$$\boldsymbol{\omega} = \frac{\hbar}{m}\boldsymbol{\nabla}^2\chi\mathbf{e}_z\,. \tag{3.24}$$

On the other hand we read off from (3.14) and (3.21) that $\omega(\mathbf{r}) = 0 for \mathbf{r} \neq 0$ and that $\int \omega(\mathbf{r}) df = \oint \mathbf{v} \cdot d\mathbf{r} = 2\pi\hbar/m$, so we conclude $\omega = 2pi\delta(\mathbf{r})$. Thus, combining this with (3.21) we get

$$\boldsymbol{\nabla}^2\chi(\mathbf{r}) = 2\pi\delta(\mathbf{r})\,. \tag{3.25}$$

Using the method of Green's function [46] we can solve (3.25) and get

$$\chi(\mathbf{r}) = \frac{1}{2\pi}\ln(|\mathbf{r}|) + C\,, \tag{3.26}$$

where we choose the integration constant such that the argument of the logarithm in (3.26) is dimensionless. Therefore we introduce the healing or coherence length ξ, which is the typical length scale for a vortex and can be interpreted as the distance at which the condensate wave function can appreciably vary or the healing of a condensate back from zero to its bulk value n_0. Mathematically this is defined as the spatial scale, where the kinetic energy per particle is equal to the interaction energy [38]

$$\frac{\hbar^2}{2m\xi^2} = n_0 g\,. \tag{3.27}$$

To get back to (3.26) we now set the integration constant to be

$$C = -\frac{1}{2\pi}\ln(\xi) \tag{3.28}$$

and get therefore the stream function

$$\chi(\mathbf{r}) = \frac{1}{2\pi}\ln\left(\frac{|\mathbf{r}|}{\xi}\right). \tag{3.29}$$

The stream function can also be interpreted geometrically, see Fig. 3.2. Thus, the gradient of the phase points in the direction of the velocity flow, whereas the gradient of the stream function points perpendicular to it. Note that also for a system with more than one vortex a suitable stream function can be found by considering the generalization of (3.25) given by [44]

$$\boldsymbol{\nabla}^2\chi(\mathbf{r}) = 2\pi\sum_{i=1}^{k} l_i\delta(\mathbf{r} - \mathbf{r}_i)\,. \tag{3.30}$$

For a complete discussion we refer to [44].

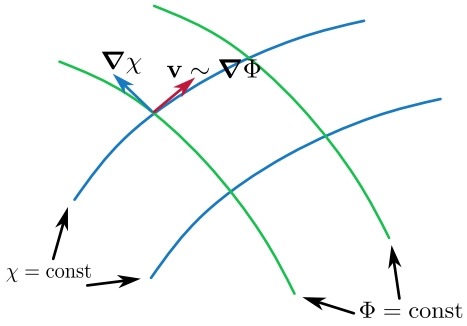

Figure 3.2.: Geometrical interpretation of the velocity field generated by a stream function in two dimensions.

3.2. Open dissipative System

After we derived in the last section the hydrodynamic description of a BEC without any particle gains or losses, we now turn our attention to the hydrodynamic description of a BEC with particle gains and losses.

3.2.1. Hydrodynamic Equations in 3D

Similar to the last section we start the derivation of the hydrodynamic equations by applying the Madelung representation to the underlying equation of motion, which is the cGPE (2.17). By separating real and imaginary parts in the upcoming equation and also using the Eqs. (3.5), (3.9) and (3.12) yields

$$\frac{\partial n}{\partial t} + \boldsymbol{\nabla}\left(n \cdot \mathbf{v}\right) = n\left(\gamma - \Gamma n\right) , \tag{3.31}$$

$$\frac{\partial \mathbf{v}}{\partial t} + \left(v \cdot \boldsymbol{\nabla}\right) v = -\boldsymbol{\nabla}\left[\frac{V}{m} + \frac{gn}{m} - \frac{\hbar^2}{2m^2}\frac{\boldsymbol{\nabla}^2\sqrt{n}}{\sqrt{n}}\right] + \left(\boldsymbol{\nabla} \times \mathbf{v}\right) \times \mathbf{v} . \tag{3.32}$$

Notice that (3.32) is exactly the same as in the closed system case (3.13). Therefore also the vorticity equation results in

$$\frac{\partial \boldsymbol{\omega}}{\partial t} + \left(\mathbf{v} \cdot \boldsymbol{\nabla}\right)\boldsymbol{\omega} = \left(\boldsymbol{\omega} \cdot \boldsymbol{\nabla}\right)\mathbf{v} - \boldsymbol{\omega} \cdot \left(\boldsymbol{\nabla} \cdot \mathbf{v}\right) . \tag{3.33}$$

Therfore the hydrodynamic equations (3.31)–(3.33) only differ from the closed system in the continuity equation (3.31). The continuity equation still describes conservation of particle density, but now with an additional right-hand side. This inhomogeneous term takes the pumping γ and losses Γ into account.
Of special interest for this thesis is the stationary state of the continuity equation (3.31). Integrating the continuity equation (3.31) yield after applying GauSS integral theorem

$$\frac{\partial N}{\partial t} = \int d\mathbf{r}\, n(\mathbf{r})\left\{\gamma - \Gamma n(\mathbf{r})\right\} . \tag{3.34}$$

Considering now an stationary state of (3.34) we therefore get

$$\int d\mathbf{r}\, n(\mathbf{r}) \left\{\gamma - \Gamma n(\mathbf{r})\right\} = 0\,. \tag{3.35}$$

Considering the homogeneous density

$$n(\mathbf{r}) = \frac{\gamma}{\Gamma} \tag{3.36}$$

and inserting this into (3.35) yields that the homogeneous density (3.36) is a solution of the stationary continuity equation.

3.2.2. Hydrodynamic Equations in 2D

As we saw in the last Section the hydrodynamic equations for an open dissipative system (3.31)–(3.33) do only differ to the closed system equation (3.10), (3.13) and (3.15) in the continuity equation. Therefore the question arises whether one can find in two dimensions, similar to section 3.1.1, a corresponding stream function. Consider to this end a system with one single-charged vortex at the origin. We know from numerical simulations and experiments in open dissipative systems like in exciton-polariton condensates [47–50] and even for photon condensates [24] that in presence of a vortex the shape of the velocity field, respectively the phase, is changed to a spiral behaviour.
Theoretically this can be described by the Helmholtz decomposition theorem [51], which states that every vector field can be decomposed into a non-divergent and a non-rotational component. Applied to the condensate velocity field gives

$$\mathbf{v}(\mathbf{r}) = \mathbf{v}_S(\mathbf{r}) + \mathbf{v}_R(\mathbf{r}) = \frac{\hbar}{m}\boldsymbol{\nabla}\varphi_S(\mathbf{r}) + \frac{\hbar}{m}\boldsymbol{\nabla}\varphi_R(\mathbf{r})\,, \tag{3.37}$$

where $\mathbf{v}_R(\mathbf{r})$ is the non-rotational component and $\mathbf{v}_S(\mathbf{r})$ is the non-divergent component. In the following we call the non-rotational velocity the regular velocity due to the fact that this component is twice continuously differentialable and therefore a regular function without any singularities. And vice versa we call the non-divergent velocity to be the singular velocity, because this component describes the circular velocity field and has therefore, as we also have seen in (3.21) a singularity.
In the following we consider similar to the closed system case a single vortex at the origin. Furthermore we assume that the singular component of the velocity field in (3.37) is equal to the closed system velocity field (3.21).
Calculating the curl of (3.37) and therefore the vorticity we get exactly the same equation (3.25) as for the closed system due to the fact that the theorem of Schwarz holds for the regular velocity. So we conclude we can analogously to the closed system define a stream function for the singular velocity, which results in (3.29). Also we can conclude that the singular velocity is not effected by pumping and dissipation and the regular velocity is not related to the charge of a vortex or the number of vortices in the system.

Therefore we assume that the singular velocity corresponds to the closed system velocity field (3.22), where we derived in Section 3.1.2 the stream function (3.26). Note that the latter fulfills by definition

$$\boldsymbol{\nabla} \cdot \mathbf{v}_S = 0\,, \tag{3.38}$$

which corresponds to the continuity equation (3.10) in the far field. So considering now the continuity equation (3.31) for the open dissipative system in the far field we get a Poisson equation for the regular velocity

$$\boldsymbol{\nabla}^2 \varphi_R = n\,(\gamma - \Gamma n)\ , \tag{3.39}$$

where the right-hand side is now a constant.
Note that the general solution of a Poisson equation of the form

$$-\Delta u(\mathbf{x}) = f(\mathbf{x}) \tag{3.40}$$

with $x \in \mathbb{R}^k$ and $f : \mathbb{R}^k \to \mathbb{R}$, does only exist according to [52], iff the right hand side in (3.40) is twice continuously differentiable and has compact support.
In our case in (3.39) the right-hand side is obviously twice continuously differentiable, but however, the only constant function with compact support in $\mathbb{R}$ is the zero-function. Therefore the Poisson equation (3.39) is not solvable by using standard thechniques.
To overcome this issue we have to use a different technique and we refer to Chapter 6.

4. Optimization Methods

Solving equations of motion analytically exact can be really hard, difficult or not even possible. So one has to construct methods to solve such equations analytically at least in an approximate way. These analytical methods are called variational or optimization methods. The main idea is to make an ansatz for the wave function depending on optimization parameters, which is close to the exact solution. Extremization of the underlying optimization equations yields then an approximate solution for the wave function.
In this chapter we introduce three different optimization methods, each applicable for a different kind of systems. As a first method we introduce the standard optimization method from Lewenstein and Zoller proposed in 1996 [**vm1996erez**], which relies on the existence of an action. Secondly, as a first optimization method for open dissipative system, we give a short introduction to the cumulant optimization method [53–55], which is based on the idea to calculate different moments for exponential like ansatz wave function. But the big disadvantage of the cumulant method is, that the method can only be applied to describe an ansatz function with a finite number of cumulants. Therefore we derive a new projection optimization method, which is based on the idea to project the underlying Hilbert space onto a parameter manifold. In this manifold one then can calculate projection optimization equations to get optimal values for the ansatz of the wave function [25].

4.1. Least Action Optimization Method

The most prominent optimization method introduced by Lewenstein and Zoller in 1996 [**vm1996erez**] is based the Hamilton or least action principle. As the name implies this method relies on the underlying action

$$\mathcal{A}\left[\psi,\psi^*\right]=\int\int dt\, d\mathbf{r}\,\mathcal{L}\,, \tag{4.1}$$

where $\mathcal{L}$ denotes the Lagrange density. Note that by extremizing the action with respect to the order parameters we get the equations of motion.
Instead of extremizing with respect to the true wave function we now make an ansatz for the wave function

$$\psi(\mathbf{r},t)\approx\Psi(\mathbf{r},\boldsymbol{\lambda}(t))\,, \tag{4.2}$$

where $\boldsymbol{\lambda}(t)=(\lambda_1(t),\lambda_2(t),...,\lambda_k(t))$ denotes a vector of yet unknown optimization parameters. Inserting the ansatz (4.2) into the action (4.1) yields an approximate action

$$\mathcal{A}\left[\psi,\psi^*\right]\approx\mathcal{A}\left[\Psi(\mathbf{r},\boldsymbol{\lambda}(t)),\Psi^*(\mathbf{r},\boldsymbol{\lambda}(t))\right]=\mathcal{A}[\boldsymbol{\lambda}(t)]\,. \tag{4.3}$$

Extremizing the approximated action (4.3) with respect to the optimization parameters $\lambda_i(t)$ leads in general to a system of coupled equations for the variational parameters

$$\frac{\delta \mathcal{A}(\boldsymbol{\lambda}(t))}{\delta \lambda_i(t')} = 0\,, \forall i \in \{1, ..., k\}\,, \tag{4.4}$$

which may be analytically solved. The big advantage of this method is that by making an approximate ansatz for the wave function we can reduce a partial differential equation to a system of ordinary differential equations.

4.2. Cumulant Method

As the standard optimization method from last section relies on the existence of an action this can not be used for open dissipative system due to the lack of particle or energy conservation. One method, which does not rely on an action is the cumulant method [53–55].
Instead of tackling the underlying equation of motion directly the cumulant method is based on statistical properties of the solution, which are called moments or cumulants. In the following we explain the procedure of the cumulant method using the example of a Gassian ansatz function, which is a valid ansatz wave function for example in a BEC described by the GPE (2.9) in presence of a harmonic trapping potential [13]. To this end we denote in this example the underlying equation of motion with EOM according to

$$EOM\left[\psi, \psi^*\right](\mathbf{r}, t) = 0\,. \tag{4.5}$$

Furthermore consider a general Gaussian ansatz in two dimensions [13]

$$\Psi = \sqrt{\frac{N}{\pi q_1(t) q_2(t)}} \exp\left(\sum_{i=1}^{2}\left[-\left(\frac{1}{2q_i(t)} + iA_i(t)\right)(r_i - r_{0i}(t))^2 + ix_i C_i(t)\right]\right). \tag{4.6}$$

To calculate now the parameters of the ansatz function we insert the latter into the equation of motion (4.5) and average this with weights f_{ik}

$$\int d\mathbf{r}\, f_{ik} \cdot \Psi^*(\mathbf{r}, \boldsymbol{\lambda}(t)) EOM\left[\psi, \psi^*\right](\mathbf{r}, \boldsymbol{\lambda}(t)) = 0\,, \tag{4.7}$$

where we used the former notation for the optimization parameters.
As we consider a Gaussian ansatz it is enough to calculate the first two cumulants, which are given by the weights [54]

$$f_{0k} = 1 \tag{4.8}$$

$$f_{1k} = r_k - r_{0k} \tag{4.9}$$

$$f_{2k} = (r_k - r_{0k})^2 - \frac{q_k^2}{2}\,, \tag{4.10}$$

where $k = 1, 2$ denotes the spatial dimension. The resulting cumulants equation of motion can now be solved either analytically or numerically yielding expressions for the optimization parameters. Note that the zeroth cumulant equation turns out to correspond to the continuity equation (3.1). Furthermore, similar to the standard optimization method, the cumulant method has the advantage to reduce a partial differential equation to a system of ordinary differential equations. However, it should be noted that the cumulant method can only be used for exponential ansatz wave functions with a finite number of cumulants and is therefore not suitable for every problem as we will see later in Chapter 6.

4.3. Projection Optimization Method

As we saw in the previous sections in case of an open dissipative system neither the standard optimization method nor the cumulant optimization method is generally applicable. Therefore we construct in this section a generially applicable optimization method, the so-called projection optimization method [25].
As a starting point we consider the space of all square integrable functions L^2, which is indeed a Hilbert space according to [30]. Furthermore we know that the complex wave function ψ solves the equation of motion

$$\mathrm{EOM}\left[\psi, \psi^*\right] = 0\,. \tag{4.11}$$

Note that for sake of simplicity we only consider one single wave function as the extension to more wave functions is straight-forward. Next we assume that the wave function ψ can be approximated by a trial function $\Psi(\boldsymbol{\lambda})$, which depends on trial parameters $\boldsymbol{\lambda}$

$$\psi(\mathbf{r}) \approx \Psi(\mathbf{r}, \boldsymbol{\lambda})\,. \tag{4.12}$$

The trial parameters can now be determined by the nonlinear algebraic equations

$$\left\langle EOM^*\left[\Psi, \Psi^*\right], \frac{\partial \Psi^*}{\partial \lambda_i} \right\rangle + \left\langle EOM\left[\Psi, \Psi^*\right], \frac{\partial \Psi}{\partial \lambda_i} \right\rangle = 0\,, \tag{4.13}$$

where $\langle \bullet, \bullet \rangle$ corresponds to the scalar product

$$\langle f, g \rangle \equiv \int d\mathbf{r}\, f(\mathbf{r}) g^*(\mathbf{r})\,. \tag{4.14}$$

Together with Riesz' representation theorem [56] and the projection theorem [57] this represents a projection from the Hilbert space L^2 onto a parameter manifold $\mathcal{M} = span(\boldsymbol{\lambda})$ spanned by the trial parameters $\boldsymbol{\lambda}$. Therefore we calculate the trial parameters not in the usual Hilbert space but in a parameter manifold $\mathcal{M}$.
The projection optimization method can also be motivated heuristically. Indeed, under the assumption some action exists, the equation of motion (4.11) corresponds to extremizing the action

$$EOM\left[\psi, \psi^*\right] = \frac{\delta \mathcal{A}}{\delta \psi^*} = 0\,. \tag{4.15}$$

Approaching the action with the wave function ansatz (4.12) the standard optimization method leads under extremization of the action with respect to the trial parameters by using the chain rule for functional derivatives [30]

$$\frac{\delta \mathcal{A}[\boldsymbol{\lambda}(t)]}{\delta \lambda_i(t')} = \int dt' \int d\mathbf{r} \left[\frac{\delta \mathcal{A}}{\delta \Psi} \frac{\delta \Psi}{\delta \lambda_i(t')} + \frac{\delta \mathcal{A}}{\delta \Psi^*} \frac{\delta \Psi^*}{\delta \lambda_i(t')} \right] = 0 \,. \tag{4.16}$$

Assuming that the ansatz wave function is a function of the optimization parameters we have

$$\frac{\delta \Psi(\mathbf{r}, t)}{\delta \lambda_i(t')} = \frac{\partial \Psi(\mathbf{r}, t)}{\partial \lambda_i(t)} \delta(t - t') \,. \tag{4.17}$$

Inserting (4.17) into (4.16) yields

$$\frac{\delta \mathcal{A}[\boldsymbol{\lambda}(t)]}{\delta \lambda_i(t')} = \int d\mathbf{r} \left[\frac{\delta \mathcal{A}}{\delta \Psi} \frac{\partial \Psi}{\partial \lambda_i} + \frac{\delta \mathcal{A}}{\delta \Psi^*} \frac{\partial \Psi^*}{\partial \lambda_i} \right] = 0 \,, \tag{4.18}$$

which corresponds to the projection optimization equations (4.13).
Note that the projection optimization method can also be geometrically illustrated as shown in the Appendix A.

5. Non-Vortex Solution

As an first example using the projection optimization method we study in this chapter the solutions of the stationary cGPE (2.18) in two dimensions in presence of an external harmonic potential

$$V(\mathbf{r}) = \frac{1}{2} m\omega^2 |\mathbf{r}|^2 \,. \tag{5.1}$$

To this end we consider separately first the established cumulant optimization method and then afterwards the newly developed projection optimization method and discuss both results.
As known from numerical studies of the stationary cGPE (2.18) in [34] (see Fig. 5.1) it is reasonable to make for small values of pumping and dissipation an approximate ansatz for the wave function in form of a Gauss profile

$$\Psi(r) = \sqrt{\frac{N}{\pi q^2}} e^{-\frac{r^2}{2q^2}} \tag{5.2}$$

with the particle number N and the width of the Gauss package q as optimization parameters. Also we are setting the center of the harmonic trap to be at the origin, so that the center of the ansatz (5.2) is also set to be at the origin.
With this ansatz (5.2) we determine in the following the optimization parameters first with the projection optimization method and afterwards using the cumulant optimization method as comparison.

5.1. Projection Optimization Solution

Calculating the equations for the particle number and the width for the Gauss profile (5.2) corresponds according to the projection optimization method (4.13) to

$$\left\langle \mathrm{EOM}\left[\Psi\right](\mathbf{r}), \frac{\partial \Psi}{\partial N} \right\rangle = \int_{\mathbb{R}^2} d\mathbf{r}\, \mathrm{EOM}\left[\Psi\right](\mathbf{r}) \frac{\partial \Psi}{\partial N} = 0 \,, \tag{5.3}$$

$$\left\langle \mathrm{EOM}\left[\Psi\right](\mathbf{r}), \frac{\partial \Psi}{\partial q} \right\rangle = \int_{\mathbb{R}^2} d\mathbf{r}\, \mathrm{EOM}\left[\Psi\right](\mathbf{r}) \frac{\partial \Psi}{\partial q} = \,. \tag{5.4}$$

Inserting the stationary cGPE (2.18) and the derivatives of the Gauss ansatz (5.2) into Eq. (5.3) yields

$$\frac{\mu}{2} - \frac{\hbar^2}{4mq^2} - \frac{m\omega^2 q^2}{2} - \frac{gN}{4\pi q^2} - i\left(\frac{\gamma}{2} - \frac{\Gamma N}{4\pi q^2}\right) = 0 \,. \tag{5.5}$$

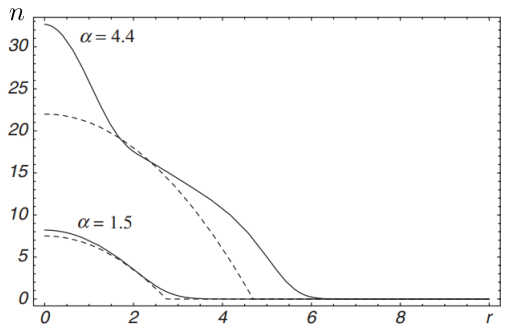

Figure 5.1.: Density n of the steady states of (2.18) for $\sigma = \Gamma/g = 0.3$ and $\alpha = 2\gamma/\hbar\omega = 1.5, 4.4$ (solid lines) and compared to the Thomas Fermi solution $n = (3\alpha/2\sigma - r^2)$ (dashed lines). Taken from [34].

Thus, because (5.5) is a complex valued equation with left hand side equal to zero and therefore the real and imaginary parts have to vanish seperatly. So separating real and imaginary part of Eq. (5.5) leads to two equations

$$\mu = \frac{\hbar^2}{2mq^2} + \frac{m\omega^2 q^2}{2} + \frac{gN}{2\pi q^2}\,, \tag{5.6}$$

$$N = \frac{2\pi\gamma q^2}{\Gamma}\,. \tag{5.7}$$

Calculating the second projection equation by inserting the stationary cGPE (2.18) and the respective derivative of the ansatz (5.2) into Eq. (5.4) yields correspondingly an equation for width q

$$q^4 = \frac{\hbar^2}{m^2\omega^2} + \frac{gN}{2\pi m\omega^2}\,. \tag{5.8}$$

With the equations (5.6)–(5.8) we thus obtain three coupled equations depending on pumping and dissipation. Solving these three equations results in the following equations for the particle number N, the width q and additionally also for the chemical potential μ

$$\tilde{\mu} = \frac{16\pi\sigma^2 + 3\alpha^2\left(1+\sqrt{1+\frac{16\pi\sigma^2}{\alpha^2}}\right)}{4\sigma^2\sqrt{16\pi^2 + \frac{2\pi\alpha^2\left(1+\sqrt{1+\frac{16\pi\sigma^2}{\alpha^2}}\right)}{\sigma^2}}}\,, \tag{5.9}$$

$$N = \frac{\alpha^2}{4\sigma^2\tilde{g}}\left[1 \pm \sqrt{1+\frac{16\pi\sigma^2}{\alpha^2}}\right]\,, \tag{5.10}$$

$$q = l_{\mathrm{osc}}\sqrt[4]{\frac{\alpha^2}{8\pi\sigma^2}\left(1+\sqrt{1+\frac{16\pi\sigma^2}{\alpha^2}}\right)+1}\,. \tag{5.11}$$

In order to make the equations clearer for understanding we introduced the oscillator leghth l_{osc} as an typical length scale for the harmonic trap.

$$l_{\mathrm{osc}} = \sqrt{\frac{\hbar}{m\omega}}\,. \tag{5.12}$$

Furthermore we also introduced the dimensionless parameters for pumping, dissipation, chemical potential and the interaction strength [34]

$$\alpha := \frac{2\gamma}{\hbar\omega}\,, \qquad \sigma := \frac{\Gamma}{g}\,, \tag{5.13}$$

$$\tilde{g} := \frac{gm}{\hbar^2}\,, \qquad \tilde{\mu} := \frac{\mu}{\hbar\omega}\,. \tag{5.14}$$

With the results (5.9),(5.10) and (5.11) we can now focus on the discussion. First of all we note that in order to have a positive particle number for every choice of pumping and dissipation the only physical relevant solution of (5.10) is the + solution. This was in fact also used in the calculations resulting in (5.9) and (5.11).
First note that all parameters in (5.9),(5.10) and (5.11) depend only on the fraction of pumping and dissipation. We see in Fig. 5.2 that every quantity is always positive, and therefore in particluar the chemical potential μ and the particle number N is indeed a thermodynamic variable [26]. Furthermore the quantities are increasing with increasing value of the fraction of pumping and dissipation. Especially considering the width (5.11) we see that this monotonously increases with the the fraction of pumping and dissipation or in case of a fixed loss rate it increases monotonously with the pumping rate α.
Of special interest is also the limit of small pumping values α by fixed losses, because usually the losses are given by the experimental setup. Therefore by expanding the chemical potential for small pumping α and fixed losses σ we get

$$\tilde{\mu} = 1 + \frac{\alpha}{2\sqrt{\pi}\sigma} + \mathcal{O}(\alpha^2)\,. \tag{5.15}$$

So we see that the chemical potential converges in the limit $\alpha, \sigma \to 0$, where $\alpha/\sigma = const$, nearly to the ground state energy $\hbar\omega/2$ of a two-dimensional harmonic oscillator. However, this does not correspond to the prediction of reference [34], in which the chemical potential in the limit of small pumping strength is given by

$$\mu \approx \frac{\hbar\omega}{2}\frac{3\alpha}{2\sigma}\,. \tag{5.16}$$

For the width of the Gauss profile, though, we get in this limit

$$q = \left(1 + \frac{\alpha}{8\sqrt{\pi}\sigma} + \mathcal{O}(\alpha^2)\right) l_{\mathrm{osc}}\,, \tag{5.17}$$

which corresponds to the width of a Gauss function in a harmonic potential and therefore matches the closed system solution well.

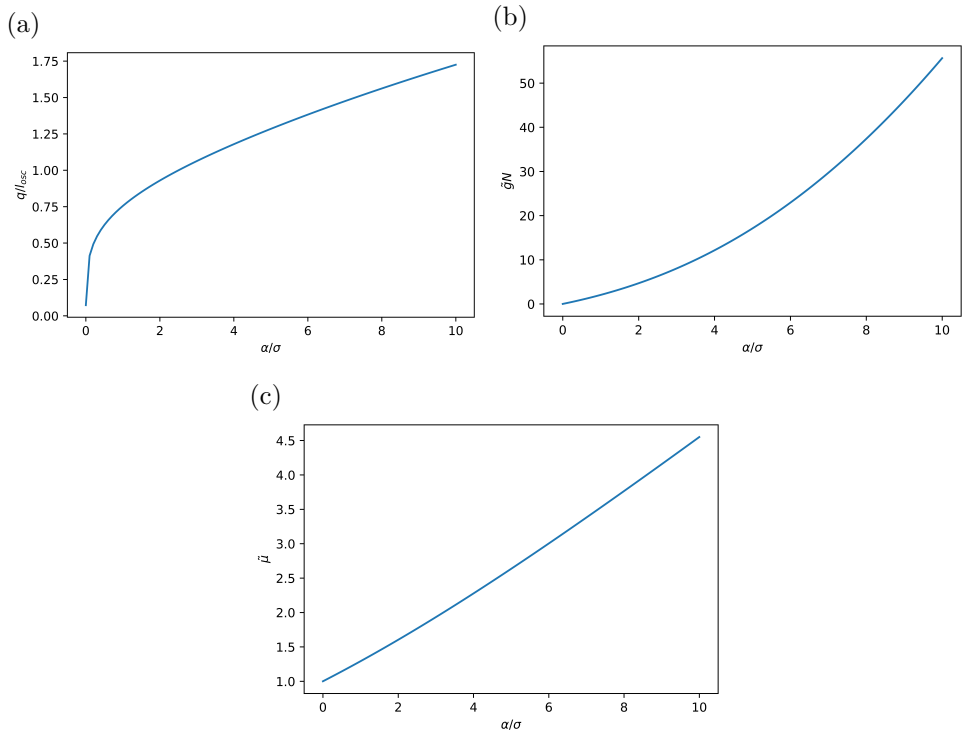

Figure 5.2.: (a) Width q of the Gauss ansatz function ploted as function of pumping α and dissipation σ in units of the oscillator length l_{osc}. (b) Particle number ploted as function of pumping α and dissipation σ in units of the dimensionless interaction strength $\tilde{g}$. (c) Chemical potential as function of pumping α and dissipation σ in units of the oscillator energy $\hbar\omega$.

5.2. Cumulant Solution

To compare the results from last section we now calculate also the cumulant optimization equations (4.7) for the particle number and the width of the Gauss profile (5.2). According to Section 4.2 it is enough to determine the zeroth and the second central moments given with the weights (4.8) and (4.10) [13]. However, due to the fact that our ansatz (5.2) for the Gauss function is centered at the origin it is not needed to also calculate the first central moment. According to Section 4.2 the zeroth cumulant equation is given by

$$\int_{\mathbb{R}^2} d\mathbf{r}\, \mathrm{EOM}\left[\Psi\right](\mathbf{r})\Psi^* = 0\,, \tag{5.18}$$

whereas the second cumulant equation refers to

$$\int_{\mathbb{R}^2} d\mathbf{r}\, \mathrm{EOM}\left[\Psi\right](\mathbf{r})\left(r^2 - \frac{q^2}{2}\right)\Psi^* = 0\,. \tag{5.19}$$

Inserting the stationary cGPE (2.18) and the Gauss ansatz (5.2) yield after performing the integrals from Eq. (5.18)

$$\frac{\mu}{2} - \frac{\hbar^2}{4mq^2} - \frac{m\omega^2 q^2}{2} - \frac{gN}{4\pi q^2} - i\left(\frac{\gamma}{2} - \frac{\Gamma N}{4\pi q^2}\right) = 0\,. \tag{5.20}$$

Similar to Eq. (5.5) calculated with the projection optimization method we seperate real and imaginary parts of (5.20), which results in

$$\mu = \frac{\hbar^2}{2mq^2} + \frac{m\omega^2 q^2}{2} + \frac{gN}{2\pi q^2}\,, \tag{5.21}$$

$$N = \frac{2\pi\gamma q^2}{\Gamma}\,. \tag{5.22}$$

Also inserting the stationary cGPE (2.18) and the Gauss ansatz (5.2), yield after performing the integrals, in Eq. (5.19)

$$q^4 = \frac{\hbar^2}{m^2\omega^2} + \frac{gN}{2\pi m\omega^2}\,. \tag{5.23}$$

However, to get this result (5.23) we use Eq. (5.22) for the particle number, causing that the imaginary part of in Eq. (5.23) vanishes.
Comparing the results obtained from the projection optimization method (5.6)–(5.8) with the cumulant optimization method (5.21)–(5.23) shows that both methods result in the same equations for the optimization parameters.
Indeed the cumulant optimization method is equivalent to the projection optimization method, which we show in the following. Calculating the needed derivatives of the Gauss ansatz (5.2) for the projection optimization method gives us

$$\frac{\partial\Psi}{\partial N} = \frac{1}{2\sqrt{N\pi q^2}} e^{-\frac{r^2}{2q^2}} = \frac{1}{2N}\Psi\,, \tag{5.24}$$

$$\frac{\partial\Psi}{\partial q} = \left(\frac{r^2}{q^3} - \frac{1}{q}\right)\sqrt{\frac{N}{\pi q^2}} e^{-\frac{r^2}{2q^2}} = \left(\frac{r^2}{q^3} - \frac{1}{q}\right)\Psi \tag{5.25}$$

Inserting Eq. (5.24) and Eq. (5.25) into the projection optimization equations for the particle number (5.3) and the width of the Gauss function (5.4)

$$\begin{aligned} 0 = \int_{\mathbb{R}^2} d\mathbf{r}\, EOM\left[\Psi\right](\mathbf{r})\,\frac{\partial\Psi^*}{\partial N} &= \int_{\mathbb{R}^2} d\mathbf{r}\, EOM\left[\Psi\right](\mathbf{r})\,\frac{1}{2N}\Psi = \\ &= \frac{1}{2N}\int_{\mathbb{R}^2} d\mathbf{r}\, EOM\left[\Psi\right](\mathbf{r})\,\Psi^*\,, \end{aligned} \tag{5.26}$$

$$\begin{aligned} 0 = \int_{\mathbb{R}^2} d\mathbf{r}\, EOM\left[\Psi\right](\mathbf{r})\,\frac{\partial\Psi^*}{\partial q} &= \int_{\mathbb{R}^2} d\mathbf{r}\, EOM\left[\Psi\right](\mathbf{r})\,\left(\frac{r^2}{q^3} - \frac{1}{q}\right)\Psi = \\ &= \frac{1}{q^3}\int_{\mathbb{R}^2} d\mathbf{r}\, EOM\left[\Psi\right](\mathbf{r})\,\left(r^2 - q^2\right)\Psi^* \end{aligned} \tag{5.27}$$

where we used the fact that our ansatz function is purely real. So the zeroth cumulant equation and the second cumulant eqution is equal to the projection optimization equations for the particle number and the width of the Gauss profile up to a global prefactor. However, this does not matter due to the fact that these equations are zero on one side

$$\int_{\mathbb{R}^2} d\mathbf{r}\, EOM\left[\Psi\right](\mathbf{r})\, \frac{\partial \Psi}{\partial N} \propto \int_{\mathbb{R}^2} d\mathbf{r}\, EOM\left[\Psi\right](\mathbf{r})\, \Psi^*\,, \tag{5.28}$$

$$\int_{\mathbb{R}^2} d\mathbf{r}\, EOM\left[\Psi\right](\mathbf{r})\, \frac{\partial \Psi}{\partial q} \propto \int_{\mathbb{R}^2} d\mathbf{r}\, EOM\left[\Psi\right](\mathbf{r})\, \left(r^2 - \frac{q^2}{2}\right) \Psi^*\,. \tag{5.29}$$

So we conclude that the projection optimization method is equivalent to the cumulant optimization method in case of a gauss ansatz function. In fact one can proof that, in case the cumulant optimization method can be applied, both optimization methods are equivalent. According to reference [13] the cumulant optimization method is also equivalent to the standard optimization method introduced in section 4.1, which we will also see in Chapter 6 for a system with a single vortex.

5.3. Solution With Complex Phase

If pumping is not that small anymore a gauss ansatz of the form (5.2) like in the previous sections is not suitable. By looking into numericalsimulations [34]we note that the density profile is denoted as a deformed Gaussian. Noticing that for increasing pumping the deformation of the Gauss profile and therefore the deviation to the Thomas Fermi profile increases, which is in [34] referred to increasing supercurrents. A reasonable way to also include the description of currents in a BEC, according to Chapter 3 and (3.5), is therefore by introducing an additional phase term to the Gauss profile

$$\Psi(\mathbf{r}) = \sqrt{\frac{N}{\pi q^2}} e^{-\frac{r^2}{2q^2} - iAr^2}\,. \tag{5.30}$$

In the optimization ansatz (5.30) we therefore include, in addition to the previous optimization parameters, an extra optimization parameter A describing the phase and therefore the strength of the currents. In the following, we therefore investigate the influence of the additional optimization parameter A on the number of particles N and the width q of the Gaussian.
Applying the projection optimization method to this problem we now have three equations to solve

$$\int_{\mathbb{R}^2} d\mathbf{r} \left\{ \mathrm{EOM}[\Psi, \Psi^*] \frac{\partial \Psi^*}{\partial N} + \mathrm{EOM}^*[\Psi, \Psi^*] \frac{\partial \Psi}{\partial N} \right\} = 0\,, \tag{5.31}$$

$$\int_{\mathbb{R}^2} d\mathbf{r} \left\{ \mathrm{EOM}[\Psi, \Psi^*] \frac{\partial \Psi^*}{\partial q} + \mathrm{EOM}^*[\Psi, \Psi^*] \frac{\partial \Psi}{\partial q} \right\} = 0\,, \tag{5.32}$$

$$\int_{\mathbb{R}^2} d\mathbf{r} \left\{ \mathrm{EOM}[\Psi, \Psi^*] \frac{\partial \Psi^*}{\partial A} + \mathrm{EOM}^*[\Psi, \Psi^*] \frac{\partial \Psi}{\partial A} \right\} = 0\,. \tag{5.33}$$

Note that we have to consider two terms in each projection optimization equation due to the fact that the ansatz function is now complex valued. Inserting the stationary cGPE (2.18) and all necessary derivatives of (5.30) needed in Eq. (5.31)–(5.33) yield after integrating the following system of coupled equations

$$N = \frac{2\pi\mu q^2}{g} - \frac{\hbar^2}{2m}\frac{2\pi}{g}\left(1 + 4A^2q^4\right) - \frac{m\omega^2\pi}{g}q^4\,, \tag{5.34}$$

$$q = \sqrt[4]{\frac{\frac{gmN}{2\pi\hbar^2}+1}{4A^2l_{\mathrm{osc}}^4+1}}\,l_{\mathrm{osc}}\,, \tag{5.35}$$

$$A = \frac{\Gamma N m}{16\pi\hbar^2 q^2} - \frac{\gamma m}{8\hbar^2}\,. \tag{5.36}$$

First we see that in the limit $A \to 0$ Eq. (5.34)–(5.36) coincide with the previous results from Eq. (5.6)–(5.8). So the results are consistent with each other. Also we can similar to the previous sections proceed further and solve this system of equations. However, this will lead to huge formulas and we will restrict oursefls for the sake of simplicity to only discuss the influence of the parameter A on the width q of the Gauss function (5.30).
To simplify the notation we introduce two length scales induced by pumping and dissipation

$$l_\gamma = \sqrt{\frac{\hbar^2}{m\gamma}}\,,\; l_\Gamma = \sqrt{\frac{\hbar^2}{mN\Gamma}}\,. \tag{5.37}$$

Furthermore we will use in the following as an abbreviation for the oscillator length

$$l_\omega = l_{\mathrm{osc}}\,. \tag{5.38}$$

Inserting (5.36) into (5.35) leads to

$$q_\pm^2 = \frac{1}{32\pi\left(\frac{l_\Gamma^2}{16l_\gamma^2} + \frac{l_\Gamma^2 l_\gamma^2}{l_\omega^4}\right)}\left\{1 \pm \sqrt{(64\pi)^2\left(\frac{\tilde{g}N}{2\pi}+1\right)\left(\frac{l_\Gamma^4}{16} + \frac{l_\Gamma^4 l_\gamma^4}{l_\omega^4}\right) - \frac{16l_\gamma^4}{l_\omega^4}}\right\}\,. \tag{5.39}$$

Demanding a, for all values of pumping and dissipation, positive width shows that only the positive solution is of physical interst. Taking the square root of (5.39) results in the equation for the width

$$q = \sqrt{\frac{1}{32\pi\left(\frac{l_\Gamma^2}{16l_\gamma^2} + \frac{l_\Gamma^2 l_\gamma^2}{l_\omega^4}\right)}\left\{1 + \sqrt{(64\pi)^2\left(\frac{\tilde{g}N}{2\pi}+1\right)\left(\frac{l_\Gamma^4}{16} + \frac{l_\Gamma^4 l_\gamma^4}{l_\omega^4}\right) - \frac{16l_\gamma^4}{l_\omega^4}}\right\}}\,. \tag{5.40}$$

Therefore we see that pumping and dissipation are directly related to the width. By increasing pumping (5.40) results also in an increasing width. Note that also for

vanishing interaction strength g the width q is still larger than the oscillator length l_ω, iff pumping and dissipation is not zero

$$q = \sqrt{\frac{1}{32\pi\left(\frac{l_\Gamma^2}{16l_\gamma^2}+\frac{l_\Gamma^2 l_\gamma^2}{l_\omega^4}\right)}\left\{1+\sqrt{(64\pi)^2\left(\frac{l_\Gamma^4}{16}+\frac{l_\Gamma^4 l_\gamma^4}{l_\omega^4}\right)-\frac{16l_\gamma^4}{l_\omega^4}}\right\}} > l_\omega \tag{5.41}$$

6. Vortex Solution

As a first example, where only the projection optimization method is applicable we consider in this chapter a homogeneous system without an external trapping potential in presence of a single vortex. Furthermore we only consider stationary states. To become more familiar with the topic of a single vortex we split the chapter in two parts. First we consider the case of a closed system with the underlying equation (2.12) and go then over to open system.

6.1. Closed System

Let us first consider in this section a single vortex in a uniform medium for a closed system. We also know that we can describe a BEC for a closed system in a stationary state with the stationary GPE (2.12). Therefore we consider in (2.12) $V = 0$ and for the sake of simplicity also a single charged vortex $l = 1$.
As a starting point we introduce the stationary state ansatz

$$\psi(\mathbf{r}, \varphi) = f(\mathbf{r})e^{i\varphi}\,, \tag{6.1}$$

which is analogous to the Madelung representation (3.4). Furthermore we rescale the amplitude of (6.1) with its bulk value f_0 and also introduce the healing length as the typical length scale for a vortex [38]. Note that from Section 2.2.2 we know that the chemical potential μ and the bulk value f_0 are related by Eq. (2.22). Inserting now the ansatz (6.1) into the stationary GPE (2.9) with the rescaled quantities yields the stationary GPE in a dimensionless form

$$-\frac{1}{r}\frac{d}{dr}\left(r\frac{d\chi}{dr}\right) + \frac{\chi}{r^2} + \chi^3 - \chi = 0\,, \tag{6.2}$$

where all spatial components are rescaled by the healing length (3.27) $r \to r/\xi$ and $\chi = f/f_0$ denotes the rescaled value of the density. Using the dimensionless GPE (6.2) we now calculate approximate solutions for the density using different types of ansatz functions.

6.1.1. Least Action Variational Method vs. Projection Optimization Method

In this section we solve the GPE with both the standard optimization method as well as with the projection optimization method using the standard literature ansatz

for the density [38]

$$\chi = \sqrt{\frac{r^2}{r^2+\alpha}}\,, \tag{6.3}$$

where the optimization parameter α has to be determined. In order to apply the standard optimization method we therefore need a quantity to extremize. One possibility is the total energy per unit length associated with the vortex [38]

$$\epsilon_V = \frac{\pi\hbar^2}{m} n_0 \int_0^D dr\, r \left\{ \left(\frac{d\chi}{dr}\right)^2 + \frac{\chi^2}{r^2} + \frac{1}{2}\left(1-\chi^2\right)^2 \right\}. \tag{6.4}$$

This total vortex energy (6.4) is thereby the difference of the total energy per unit length of the uniform system and the energy per unit length along the vortex axis (6.4). Note that we have to introduce an ultraviolet cutoff due to the divergence of the vortex energy (6.4) in a uniform medium [38]. This quantity (6.4) can now be used in the standard optimization method.
Inserting the density ansatz (6.3) into the vortex energy (6.4) leads to

$$\epsilon_V = \int_0^D dr \left\{ r\left(\frac{1}{\sqrt{r^2+\alpha}} - \frac{r^2}{\sqrt{r^2+\alpha}^3} \right)^2 + \frac{r}{r^2+\alpha} + \frac{r}{2}\left(1 - \frac{r^2}{r^2+\alpha}\right)^2 \right\}. \tag{6.5}$$

Using partial integration and simple substitutions in (6.5) leads to the following approximation of the vortex energy

$$\epsilon_V = \frac{1}{4} - \frac{\alpha^2}{4\left(\alpha+D^2\right)^2} + \frac{1}{2}\ln\left(1+\frac{D^2}{\alpha}\right) + \frac{\alpha}{4} - \frac{\alpha^2}{4\left(\alpha+D^2\right)}\,, \tag{6.6}$$

where we also directly note that in the limit $D \to \infty$ the energy (6.6) diverges. Minimizing (6.6) with respect to the optimization parameter α results in

$$\frac{d\epsilon_V}{d\alpha} = \frac{\alpha^2-2\alpha}{4\left(\alpha+D^2\right)^2} + \frac{\alpha^2}{2\left(\alpha+D^2\right)^3} - \frac{2\alpha}{4\left(\alpha+D^2\right)} - \frac{D^2}{2\alpha\left(\alpha+D^2\right)} + \frac{1}{4} \stackrel{!}{=} 0\,, \tag{6.7}$$

where we now can explicitly take the limit $D \to \infty$ leading to

$$-\frac{1}{2\alpha} + \frac{1}{4} = 0 \;\Leftrightarrow\; \alpha = 2 \tag{6.8}$$

As a comparison to the standard optimization method we now calculate the value of α using the projection optimization method. Therefore according to Chapter 4 the following projection optimization equation has to be solved

$$\int_{\mathbb{R}^2} d\mathbf{r}\, \mathrm{EOM}\left[\chi\right](\mathbf{r}) \frac{\partial\chi}{\partial\alpha} = 0\,. \tag{6.9}$$

Inserting the ansatz (6.3) into the projection optimization equation (6.9) leads to

$$\lim_{D\to\infty}\int_0^D dr\left\{\frac{4r^3}{\left(r^2+\alpha\right)^3}+\frac{r^5}{\left(r^2+\alpha\right)}^3-\frac{3r^5}{\left(r^2+\alpha\right)^4}-\frac{r^3}{\left(r^2+\alpha\right)^2}\right\}=0\,. \tag{6.10}$$

Note that also here an ultraviolet cutoff was introduced due to the divergence of the integral. Performing all integrals yields

$$0=\lim_{D\to\infty}\left\{\frac{\alpha^2}{2\left(D^2+\alpha\right)^3}-\frac{\alpha}{2\left(D^2+\alpha\right)^2}-\frac{\alpha^2-2\alpha-2}{4\left(D^2+\alpha\right)}+\frac{1}{2\alpha}-\frac{1}{4}\right\}=\frac{1}{2\alpha}-\frac{1}{4}\,, \tag{6.11}$$

where the limit $D\to$ can now be taken. Therefore we also get corresponding to the projection optimization method the same result as with the standard optimization method (6.8)

$$\alpha=2\,. \tag{6.12}$$

This result for the approximate density can be now compared with numerical simulations. To obtain numerical results by using python we therefore apply to the GPE (6.2) a 4th order collocation algorithm [58] already implemented by the function 'solve_bvp'. Using this algorithm requires a boundary value problem and therefore we are using for the density profile Dirichlet boundary conditions. Comparing the approximate result with the numerical solution as we can see in Fig. 6.1 already the standard literature ansatz (6.3) matches good with the numerical simulation. Although we see that the ansatz (6.3) crosses the numerical solution such that the approximation is larger than the numerical solution for small r and becomes smaller for larger r. Furthermore we note that the approximate solution matches the numerics for large distances, but approximates the numerics for smaller distances only moderately. Therefore the question arises, if there are better fitting ansatz functions approximating better also smaller distances.

6.1.2. Alternative Optimization Ansatzes

From a numerical simulation, as shown in Fig. 6.1, we also can think of different ansatz functions, which might fit better the true solution. Therefore we consider in this section two different types of ansatzes. The first ansatz we consider is an exponential ansatz function with one optimization parameter β and the second we consider is an ansatz function in form of a hyperbolic tangens with also one optimization parameter δ

$$\chi_\beta=1-e^{-\beta r}\,, \tag{6.13}$$

$$\chi_\delta=\tanh(\delta r)\,. \tag{6.14}$$

Starting with the exponential ansatz function (6.13) and calculate the vortex energy (6.4) yields the following integral equation

$$\epsilon_V=\int_0^D dr\left\{\beta^2 r e^{-2\beta r}+\frac{1}{r}\left(1-e^{-\beta r}\right)^2+\frac{r}{2}\left(1-\left(1-e^{-\beta r}\right)^2\right)^2\right\}\,. \tag{6.15}$$

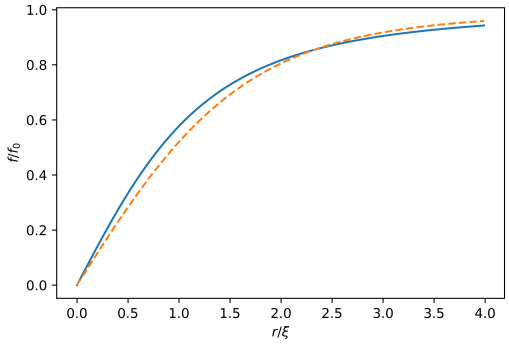

Figure 6.1.: The rescaled amplitude of the wave function as function of r. The dashed line represents the numerical solution of (6.2) and the straight line denotes the approximate solution (6.3), (6.12) obtained with both optimization methods.

Evaluating the integrals as shown in the Appendix B leads to

$$\begin{aligned}\epsilon_V =& \frac{1}{4} + \gamma + \ln\left(\frac{D\beta}{2}\right) - \frac{\beta^2 + 2\beta^2 D + 4\beta D + 2}{4\beta^2} e^{-2\beta D} + \frac{2 + 6\beta D}{9\beta^2} e^{-3\beta D} \\ & - \frac{1 + 4\beta D}{32\beta^2} e^{-4\beta D} + \frac{89}{288\beta^2} + \sum_{k=0}^{n} \left\{ \frac{(-1)^k\, k!}{(\beta D)^{k+1}} \left(2e^{-\beta D} - \frac{1}{2k+1} e^{-2\beta D} \right) \right\} ,\end{aligned} \tag{6.16}$$

where γ denotes the Euler-Mascheroni constant. For further information concerning the evaluation of the integrals we refer to Appendix B.
Minimizing the energy (6.16) with respect to the optimization parameter β yields the limit

$$\lim_{D\to\infty} \frac{d\epsilon_V}{d\beta} = \frac{1}{\beta} - \frac{89}{144\beta^3} \stackrel{!}{=} 0 \Leftrightarrow \beta = \pm\sqrt{\frac{89}{144}} \,. \tag{6.17}$$

Note that only the positive solution is physical relevant, because the negative solution yields an exponentially increasing density.

In the second part of this section we consider the ansatz (6.14) and calculate at first the vortex energy (6.4)

$$\epsilon_V = \int_0^D dr \left\{ r\delta \left[1 - \tanh^2(\delta r)\right] + \frac{\tanh^2(\delta r)}{r} + \frac{r}{2} \left[1 - \tanh^2(\delta r)\right]^2 \right\} . \tag{6.18}$$

Evaluating the integrals yields according to Appendix B

$$\begin{aligned}\epsilon_V =& \tanh(\delta D) \frac{D - 6\delta D}{2\delta} - \tanh^3(\delta D) \frac{2\delta D + D}{6\delta} + \ln(\cosh(\delta D)) \frac{2\delta + 1}{3\delta^2} \\ & + \frac{1}{\cosh^2(\delta D)} \frac{2\delta + 1}{12\delta^2} + \frac{2\delta + 1}{12\delta^2} + \ln(\delta D) + R \,,\end{aligned} \tag{6.19}$$

where R is a numerical constant given by

$$R = \int_0^1 dx \left\{ \frac{\tanh(x)}{x} + \frac{4}{x\left(e^{2x}+1\right)^2} - \frac{4}{x\left(e^{2x}+1\right)} \right\} \approx 0,2095\,. \tag{6.20}$$

For further information we refer also here to Appendix B. Taking the derivative of (6.19) with respect to δ yields

$$\begin{aligned} \frac{d\epsilon_V}{d\delta} =& D\left(1-\tanh^2(\delta D)\right)\frac{D-10\delta D}{3\delta} + \tanh(\delta D)\frac{2D}{3\delta} - \ln(\cosh(\delta D))\frac{4}{3\delta^2} + \\ &+ \operatorname{sech}^2(\delta D)\left[-\frac{\delta+1}{6\delta^3} + D\left(1-\tanh^2(\delta D)\right)\frac{2\delta D+D}{6\delta} - \tanh(\delta D)\frac{D}{6\delta^2}\right] \\ &- 2D\operatorname{sech}^2(\delta D)\tanh(\delta D)\left[\frac{2\delta+1}{12\delta^2} + \tanh(\delta D)\frac{2\delta D+D}{6\delta}\right] + \frac{6\delta^2-\delta-1}{6\delta^3}\,, \end{aligned} \tag{6.21}$$

wwhere we now can perform the limit $D \to$. To this end we are using also the formula for the limit

$$\lim_{D\to\infty}\left\{\ln(\cosh(\delta D)) - \delta D\tanh(\delta D)\right\} = \ln\left(\frac{1}{2}\right). \tag{6.22}$$

Thus this yields a polynomial of third order for the optimization parameter δ

$$3\delta^3 + \frac{1}{2}\delta^2 + \left(\frac{1}{2} + \ln\left(\frac{1}{2}\right)\right)\delta + \ln\left(\frac{1}{2}\right) = 0\,. \tag{6.23}$$

Solving (6.23) leads to two solutions

$$\delta_1 \approx 0.595\,, \tag{6.24}$$

$$\delta_2 \approx -0.381\,, \tag{6.25}$$

where the solution (6.25) is not of physical interest, because this would lead to a negative density profile.

6.1.3. Discussion

In this section we compare the optimization results for the different ansatz functions (6.3) with $\alpha = 2$, (6.13) with $\beta = \sqrt{\frac{89}{144}}$ and (6.14) with $\delta = 0,595$ with the numerical solution of (6.2), see Fig. 6.2. First we note that all found approximations match quite well with the numerical result. However, all results also cross the numerical solution. Furthermore the approximations match the numerics for large distances quite well and yield therefore a good description far away from the vortex. Nevertheless, it is noticeable that the exponential approach (6.13) describes the numerical solution much faster than the other two ansatzes for the far field. Furthermore, when considering the near field, the hyperbolic tangent ansatz (6.14) best approximates the numerical solution. From this we can conclude that the hyperbolic tangent ansatz (6.14) is best for analysing the near field of the vortex and the exponential ansatz (6.13) for describing the far field.

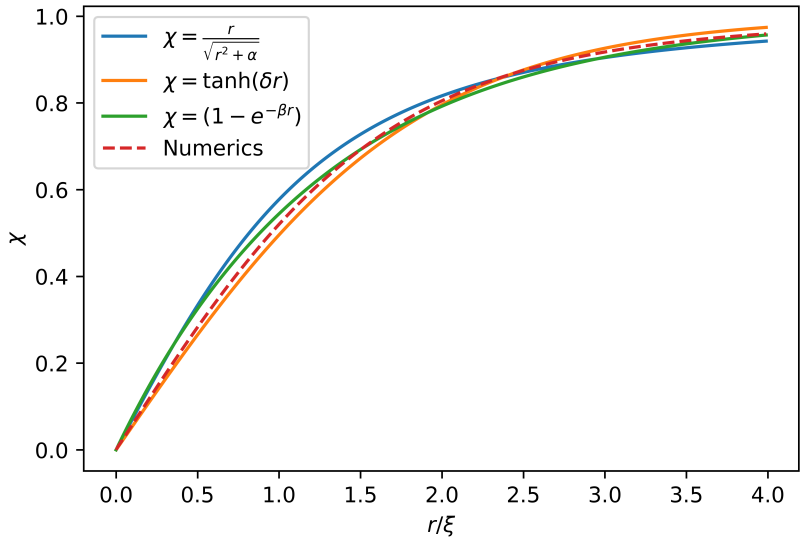

Figure 6.2.: Rescaled density plotted as function of r for the different ansatz functions compared with the numerical solution of (6.2).

6.2. Open Dissipative System

In this Section we go now from the closed system to the open dissipative system case. The goal in the following calculations is to get a first insight of the analytical description of a single charged vortex in a stationary state for open dissipative systems. As we already introduced in Section 1.3 the main differnce between a vortex in a closed system and the open dissipative system lies in the velocity field, which has now, as shown in [24, 59] from numerical investigations, a spiral shape. To this end, we consider the stationary cGPE (2.18) and apply the transformation

$$\Psi(\mathbf{r}) = \sqrt{n_0} f(|\mathbf{r}|) e^{i\Phi(|\mathbf{r}|,\varphi)} \,. \tag{6.26}$$

Note that the representation for the open system (6.26) and the representation for the closed systems (6.1) are quite similar. However, the two representations differ fundamentally in the phase of the wave function, which has in case of an opoen dissipative system also a spatial component. Due to the spiral shape of the velocity field induced by the vortex we are using the Helmholtz vector decomposition theorem [51] to decompose the velocity field into a non-rotational and a non-divergent part, similar to (3.37) from Section 3.2.2, yielding

$$\mathbf{v}(r,\varphi) = \mathbf{v}_S(\varphi) + \mathbf{v}_R(r) \,. \tag{6.27}$$

Due to the relation (3.5) between the velocity field and the phase of the condensate it follows directly from (6.27) that the phase Φ can also be decomposed into two components

$$\Phi(r,\varphi) = \varphi_S(\varphi) + \varphi_R(r) \,, \tag{6.28}$$

where φ_S denotes the circular component, which we also refer like in Section 3.2.2 to be the singular phase, and φ_R represents the radial contribution of the phase, which we refer to be the regular phase. Furthermore we know from the hydrodynamic chapter that the open dissipative parameters only influence the regular velocity (3.39). Therefore we assume that the singular phase and the singular velocity to be the same as in the closed system

$$\varphi_S(\varphi) = \varphi \;\Rightarrow\; \mathbf{v}_S = \frac{\hbar}{m}\boldsymbol{\nabla}\varphi_S = \frac{\hbar}{m}\frac{\mathbf{e}_\varphi}{r}\,. \tag{6.29}$$

However, as calculated in Section 3.2.2 we can not continuity equation for the open dissipative system exactly without taking into account the density profile. Therefore we determine in the following an analytical approach using the projection optimization method [25]. To this end we make the standard literature density ansatz (6.3) for closed systems. Note that at this point we are not able to also make an ansatz for the velocity field. Solving the stationary cGPE (2.18) can be done in two different but equivalent ways.
One possibility is to separate the real and imaginary part of the stationary cGPE (2.18). To this end we insert (6.26) into the cGPE (2.18) and then separate real and imaginary parts, which leads to

$$0 = \mu + \frac{\hbar^2}{2m}\left[\frac{\boldsymbol{\nabla}^2 f}{f} - \frac{1}{r^2} - \left(\boldsymbol{\nabla}\varphi_R\right)^2\right] - g n_0 f^2\,, \tag{6.30}$$

$$0 = \frac{\hbar^2}{2m}\left[\boldsymbol{\nabla}^2\varphi_R + 2\frac{\boldsymbol{\nabla} f}{f}\cdot\boldsymbol{\nabla}\varphi_R\right] - \frac{1}{2}\left[\gamma - \Gamma n_0 f^2\right]\,. \tag{6.31}$$

Note that for large distances according to Section 3.2.2 the chemical potential μ, the density n_0, the pumping γ and the losses Γ are related by (2.22). Also we see that using $\sqrt{n_0}f = \sqrt{n}$ that Eq. (6.31) corresponds to the continuity equation (3.31) and Eq. (6.30) to the velocity equation (3.32) in a steady state.
Inserting the ansatz (6.3) into the Eq. (6.31) yields a second order ordinary differential equation, which can be solved analytically exact dependent on the trial parameter α. To determine the optimal value for the trial parameter α we can use to this end the projection optimization method applied to Eq. (6.30).
However, in this section we show a different possibility by solving the whole stationary cGPE (2.18). First combining the density ansatz (6.3) and the separation of the phase components (6.28) with the transformation (6.26) yields an ansatz for the wave function Ψ

$$\Psi(\mathbf{r}) = \sqrt{n_0}\sqrt{\frac{r^2}{r^2+\alpha}}e^{i\varphi + i\varphi_R(r)}\,. \tag{6.32}$$

This ansatz we now use in the projection optimization method to find an approximate solution to the stationary cGPE (2.18). Treating the radial phase φ_R as an optimization trial function leads to the projection optimization equation

$$\int_{\mathbb{R}^2} d\mathbf{r}\left\{\mathrm{EOM}(\mathbf{r})\left[\Psi,\Psi^*\right]\frac{\delta\Psi^*(\mathbf{r})}{\delta\varphi_R(\mathbf{r}')} + \mathrm{EOM}^*(\mathbf{r})\left[\Psi,\Psi^*\right]\frac{\delta\Psi(\mathbf{r})}{\delta\varphi_R(\mathbf{r}')}\right\} = 0\,. \tag{6.33}$$

Using the functional chain rule applied to the wave function ansatz (6.32)

$$\frac{\delta\Psi(\mathbf{r})}{\delta\varphi_R(\mathbf{r}')} = \frac{\partial\Psi(\mathbf{r})}{\partial\varphi(\mathbf{r})}\frac{\delta\varphi_R(\mathbf{r})}{\delta\varphi_R(\mathbf{r}')} = i\Psi(\mathbf{r})\delta(\mathbf{r}-\mathbf{r}') \tag{6.34}$$

$$\frac{\delta\Psi^*(\mathbf{r})}{\delta\varphi_R(\mathbf{r}')} = \frac{\partial\Psi^*(\mathbf{r})}{\partial\varphi(\mathbf{r})}\frac{\delta\varphi_R(\mathbf{r})}{\delta\varphi_R(\mathbf{r}')} = -i\Psi^*(\mathbf{r})\delta(\mathbf{r}-\mathbf{r}') \tag{6.35}$$

results due to the definition of the delta-distribution to a vanishing spatial integral. Therefore this leads to a second order inhomogeneous ordinary differential equation for the singular phase

$$\frac{d^2\varphi_R}{dr^2} + \frac{r^2+3\alpha}{r\,(r^2+\alpha)}\frac{d\varphi_R}{dr} = \frac{\gamma m}{\hbar^2}\frac{\alpha}{r^2+\alpha}\,. \tag{6.36}$$

Note that we used in (6.33) the relation $n_0 = \gamma/\Gamma$ between pumping, dissipation and the bulk value for the density. Therefore the only parameter of the open dissipative system, which is involved in the singular phase is the pumping rate γ. Furthermore reducing the order of (6.33) by introducing the quantity

$$v_R(r) = \frac{d\varphi_R(r)}{dr} \tag{6.37}$$

yields a first order inhomogeneous ordinary differential equation for v_R. Note that due to (3.5) the quantity v_R is proportional to the absolute value of the regular velocity:

$$\frac{dv_R}{dr} + \frac{r^2+3\alpha}{r\,(r^2+\alpha)}v_R = \frac{\gamma m}{\hbar^2}\frac{\alpha}{r^2+\alpha}\,. \tag{6.38}$$

The general solution of such a differential equation (6.38) is according to [60] a superposition of the homogeneous solution and one particular solution. Therefore the general solution of (6.38) has the form

$$v_R(r) = v_R^{\mathrm{hom}}(r) + v_R^{\mathrm{part}}(r)\,. \tag{6.39}$$

In order to find these solutions let us first consider a generalization of (6.38)

$$\frac{du(x)}{dx} + a(x)u(x) = b(x)\,, \tag{6.40}$$

where $u(x)$ is a general function fulfilling the differential equation (6.40) and $a(x), b(x)$ are arbitrary but continuous functions.
The general solution of the homogeneous case is then given by

$$u^{\mathrm{hom}}(x) = C\exp\left(-\int dx\, a(x)\right), \tag{6.41}$$

where C is a integration constant and determined by boundary conditions. Via separation of constants one also finds the particular solution, which is given by

$$u^{\mathrm{part}}(x) = \left[\int b(x)e^{\int a(x)dx}dx\right]e^{-\int a(x)dx}\,. \tag{6.42}$$

With these equations we can now determine the homogeneous solution and the particular solution of (6.38) leads after integration to

$$v_R^{\mathrm{hom}}(r) = C\frac{r^2+\alpha}{r^3}\,, \tag{6.43}$$

$$v_R^{\mathrm{part}}(r) = \frac{\alpha\gamma m}{2\hbar^2}\left[\ln\!\left(r^2+\alpha\right)\frac{r^2+\alpha}{r^3}+\frac{\alpha}{r^3}\right]. \tag{6.44}$$

Therefore the general solution is given by

$$v_R(r) = C\frac{r^2+\alpha}{r^3}+\frac{\alpha\gamma m}{2\hbar^2}\left[\ln\!\left(r^2+\alpha\right)\frac{r^2+\alpha}{r^3}+\frac{\alpha}{r^3}\right]. \tag{6.45}$$

To determine the integration constant we impose Dirichlet boundary conditions for v_R, .e. v_R must vanish at the origin.. By expanding the general solution (6.45) for small r leads to the value of the integration constant C

$$C = -\frac{\alpha\gamma m}{2\hbar^2}\left[1-\ln(\alpha)\right]. \tag{6.46}$$

Inserting the found constant (6.46) into the general solution (6.45) yields

$$v_R(r) = \frac{\alpha\gamma m}{2\hbar^2}\left[\ln\!\left(\frac{r^2+\alpha}{\alpha}\right)\frac{r^2+\alpha}{r^3}-\frac{1}{r}\right], \tag{6.47}$$

which we also can rewrite in terms of the healing length ξ

$$v_R(r) = \frac{1}{\xi^2}\frac{\alpha\gamma}{4\mu}\left[\ln\!\left(\frac{r^2+\alpha}{\alpha}\right)\frac{r^2+\alpha}{r^3}-\frac{1}{r}\right]. \tag{6.48}$$

Note that with the choice of the integration constant the velocity field also fulfills automatically Dirichlet boundary conditions at infinity. To calculate the trial optimization parameter α according to the projection optimization method leads to the projection optimization equation

$$\int_{\mathbb{R}^2} d\mathbf{r}\left\{\mathrm{EOM}\left[\Psi,\Psi^*\right](\mathbf{r})\frac{\partial\Psi^*(\mathbf{r})}{\partial\alpha}+\mathrm{EOM}^*\left[\Psi,\Psi^*\right](\mathbf{r})\frac{\partial\Psi(\mathbf{r})}{\partial\alpha}\right\}=0 \tag{6.49}$$

Inserting the ansatz for the wave function (6.32) yields after integration the intermediate result for the trial parameter α

$$\frac{\hbar^2}{2m}\int_0^\infty dr\frac{r^3}{\left(r^2+\alpha\right)^2}v_R^2(r) = \frac{g\gamma}{4\Gamma}-\frac{\hbar^2}{4m\alpha}\,. \tag{6.50}$$

Note that in the limit $v_R\to 0$ by using (2.22) the Eq. (6.50) results directly to the value of the trial parameter α for the closed system case

$$\frac{g\gamma}{4\Gamma}-\frac{\hbar^2}{4m\alpha}=0 \;\Leftrightarrow\; \alpha = 2\xi^2\,. \tag{6.51}$$

In order to evaluate (6.50) further we insert the solution of the radial velocity (6.48), which leads to

$$\alpha^2 - \frac{4g\hbar^2}{\Gamma\gamma m}\alpha + \left(\frac{2\hbar^2}{\gamma m}\right)^2 = 0\,. \tag{6.52}$$

Solving the quadratic equation (6.52) for α leads to two solutions

$$\alpha_\pm = 4\frac{\mu}{\gamma}\frac{g}{\Gamma}\left[1 \pm \sqrt{1 - \left(\frac{\Gamma}{g}\right)^2}\right]\xi^2\,. \tag{6.53}$$

Note that demanding in the closed system limit $\Gamma \to 0$ only the $-$-solution is of physical interest. Also we notice that for increasing loses Γ the square root in (6.53) becomes imaginary and therefore we get, by demanding a real valued density, a restriction for the possible values of losses

$$0 \leq \left|\frac{\Gamma}{g}\right| \leq 1\,. \tag{6.54}$$

Using the relation between losses and pumping in a steady state (2.22) we therefore also get a restriction for the pumping parameter

$$0 \leq \left|\frac{\gamma}{\mu}\right| \leq 1\,. \tag{6.55}$$

As shown in Fig. 6.3 a) the value of the optimization parameter α increases by increasing the loss rate Γ up to $\Gamma/g = 1$, because increasing further would lead to a complex value of α. Also we see in Fig. 6.3 that depending on the observation area the velocity field has different types of behaviour. Near the vortex core, the velocity field is mostly circular similar to the closed system. At some intermediate distance from the vortex we see the spiral behaviour and at large distances the radial component dominates the circular motion such that the velocity field is mostly radial, as shown in Fig. 6.3.

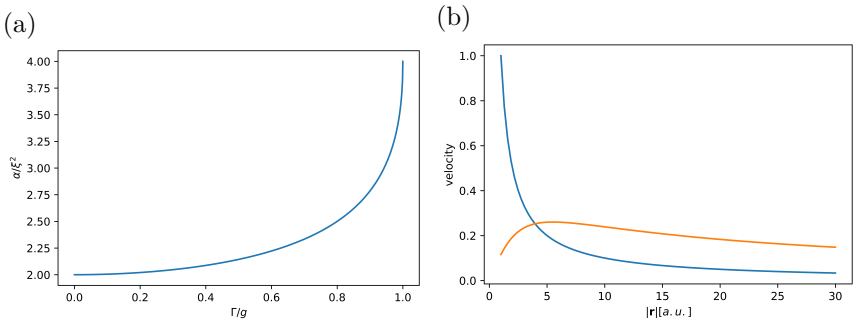

Figure 6.3.: Left: Optimization parameter α as a function of losses Γ. Right: Comparison of radial velocity (orange) with singular velocity (blue) as a function of r

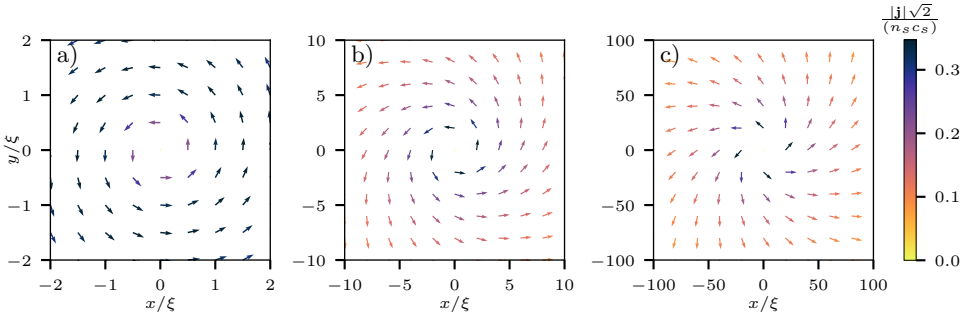

Figure 6.4.: Current $|\mathbf{j}| = \hbar\,\mathrm{Im}(\psi\boldsymbol{\nabla})\psi^*)$ around vortex with $\Gamma/g = 0.4$. From left to right different characteristics are visible depending on the observation area.

6.3. Discussion and Numerical Simulation

In order to compare the analytical results from the previous section, we now also solve numerically the cGPE (2.17). Therefore it is helpful to write the cGPE (2.17) in dimensionless units. According to [25] we rescale the particle density with the saturation density n_0 and choose as the characteristic length scale the healing length ξ from (3.27) to rescale all length units as well as $\xi\sqrt{2}/c_0$ for time units, where c_0 denotes the sound velocity [61]. With this we get

$$i\frac{\partial\psi}{\partial t} = \left[-\boldsymbol{\nabla}^2 + |\psi|^2 + \frac{i}{2}\sigma\left(1 - |\psi|^2\right)\right]\psi\,. \tag{6.56}$$

Note that Eq. (6.56) only depends on one parameter $\sigma = \Gamma/g$ describing the losses in the system.
Applying the pseudospectral method [62] to the dimensionless cGPE (6.56) together with the simulator XMDS2 [63] yields then a numerical solution. To do the time steps we are using 4th order adaptive Runge-Kutta method with step size $h_t = 10^{-5}$.

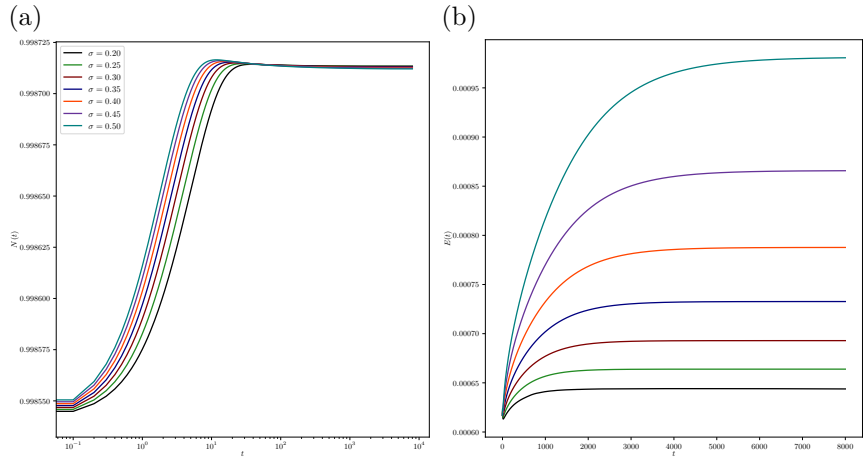

Figure 6.5.: Left: Particle number as function of time. Right: Energy as function of time. In both figures are plotted the quantities for different values of losses.

To solve the spatial part we implement a cosine basis and use a square box of size $L = 400$ with a grid size of $h_x = h_y = 0.5$. The reason for choosing the cosine basis is that this automatically imposes Neumann boundary conditions at the edges of the box.
Furthermore to prepare an initial state of the wave function we are using the analytically approximated density solution of the closed system case (6.3) with the calculated optimization parameter (6.12)

$$\Psi_{\text{init}}(r, \varphi) = \frac{r}{\sqrt{r^2 + 2}} e^{i\varphi} \,. \tag{6.57}$$

Therefore we put a single charged vortex in the center of the integration box as an initial state. To reach a stationary state we have to fulfill the steady state continuity equation (3.35). Therefore we consider in the simulation the particle number and the energy in the system and apply the condition for a steady state

$$\frac{\partial N}{\partial t} = 0 \,. \tag{6.58}$$

$$\frac{\partial E}{\partial t} = 0 \,. \tag{6.59}$$

Note that in the closed system case both conditions are equivalent, but however, for an open dissipative system we have to consider both as they are not simultaneously fulfilled, as Fig. 6.5 shows. Furthermore due to the used numerical method and starting with the closed system vortex solution as an initial state, we see in Fig. 6.6 and Fig. 6.7 that the spiral behaviour of the phase becomes more visible for increasing time. Therefore we see that the radial velocity has to propagate from the origin through the whole system until it reaches the walls of the box. With the ob-

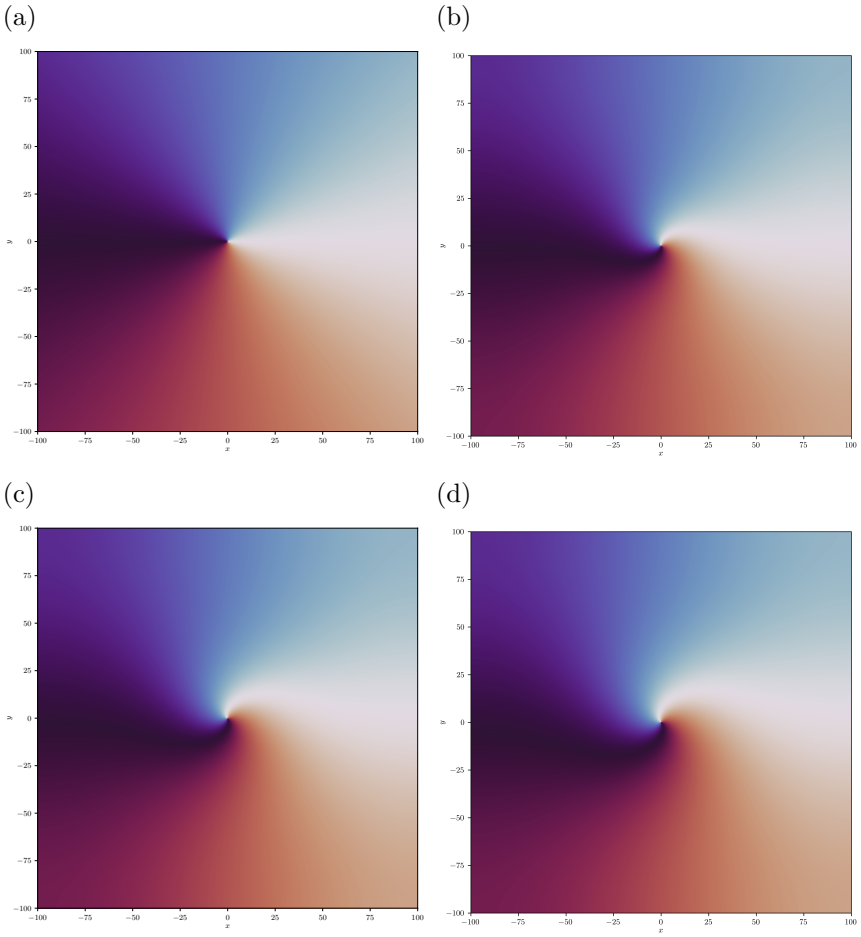

Figure 6.6.: Evolution of the phase in two dimensions. Starting in a) for t=0, b) t=250, c) t=500, d) t=750.

tained numerical results for the system in a steady state we can finally compare the approximate analytical solutions obtained in Section 6.2 with the numerical data. As shown in Fig. 6.8 the analytical solution for the velocity field agrees excellent with the numerical results. Comparing also the density profiles leads to a very good match, as shown in Fig. 6.9. Although the analytical approach only differes noticeably from the numerical data in the intermediate distance, which is only visible in an magnification of the area. This can be understood by considering equation (6.30) as the density is only affected pertubatively by the dissipation dependence of the velocity field. However, considering also the comparison of the radial velocity field we notice a larger deviation between numerics and the result obtained by the projection optimization method by increasing the loss rate Γ/g, see Fig. 6.10. This is also noticeable in the maximum value of the radial velocity and the the optimization parameter α as shown in Fig. 6.11.

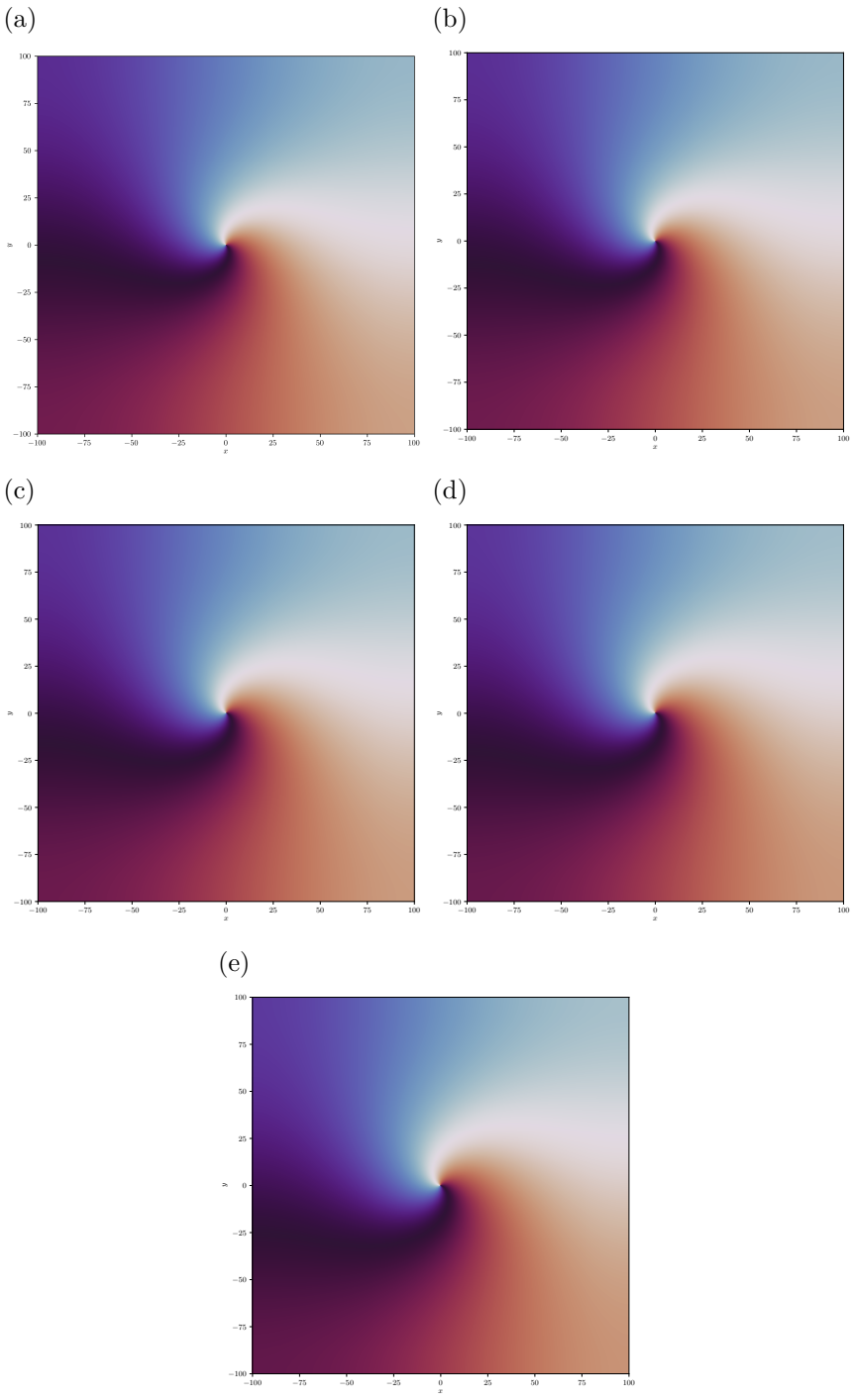

Figure 6.7.: Evolution of the phase in two dimensions. Starting in a) t=1000, b) t=1250, c) t=1500, d) t=1750, e) t=2000.

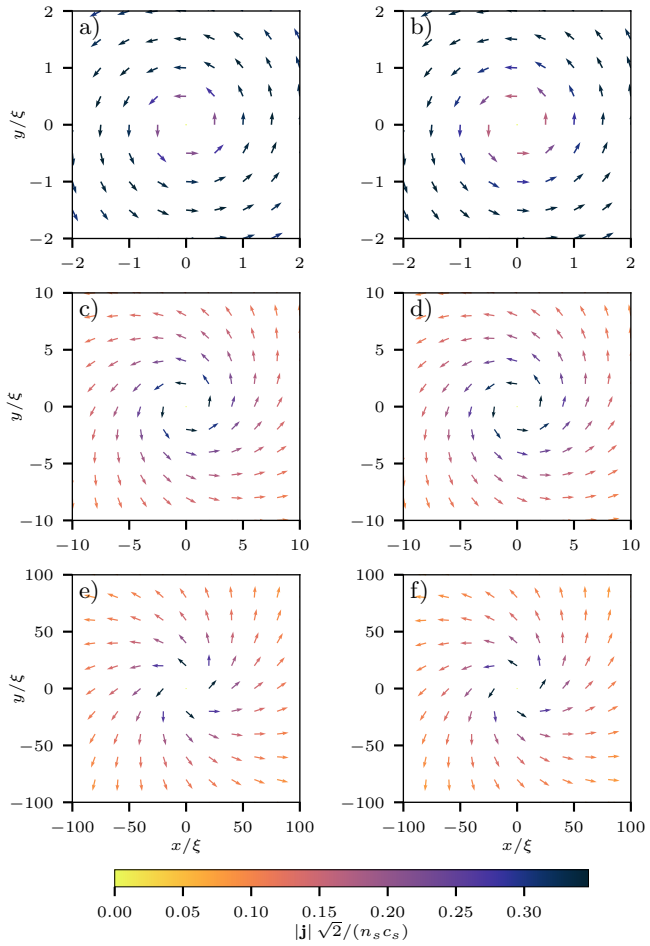

Figure 6.8.: Current $|\mathbf{j}| = \hbar\,\mathrm{Im}(\psi\boldsymbol{\nabla})\psi^*)$ around vortex with $\Gamma/g = 0.4$. Left column is the calculated analytical solution. Right column is the corresponding numerical result. Taken from [25].

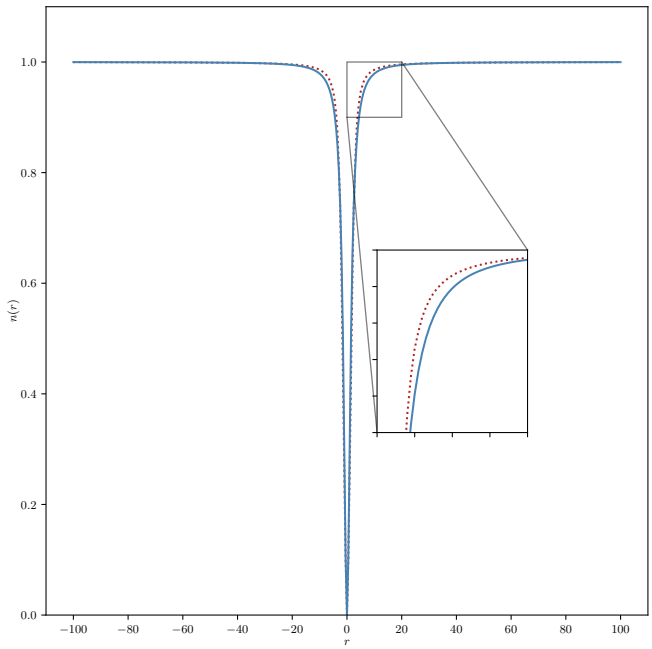

Figure 6.9.: Density profile for a loss rate $\Gamma/g = 0.5$. The dotted line represents the numerical solution, whereas the straight line corresponds to the projection optimization approach. Taken from [25].

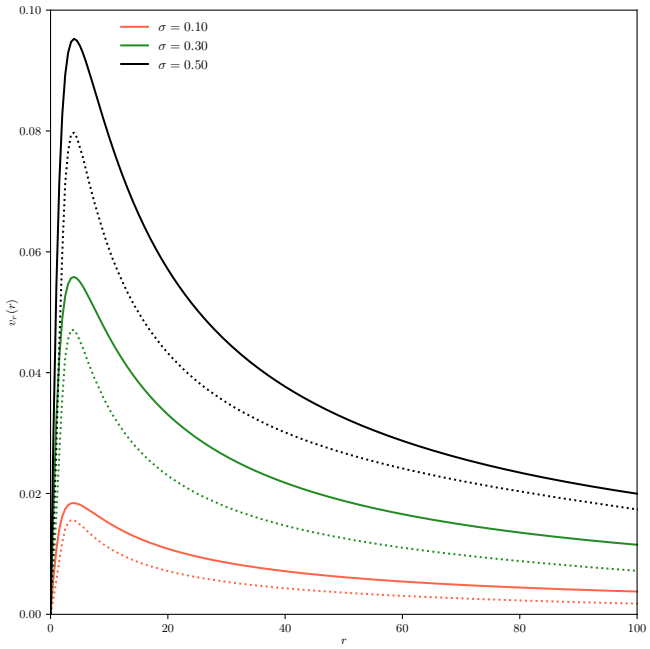

Figure 6.10.: Radial velocity for different values of losses. The dotted lines represent the numerical solution, whereas the straight line corresponds to the projection optimization approach. Taken from [25].

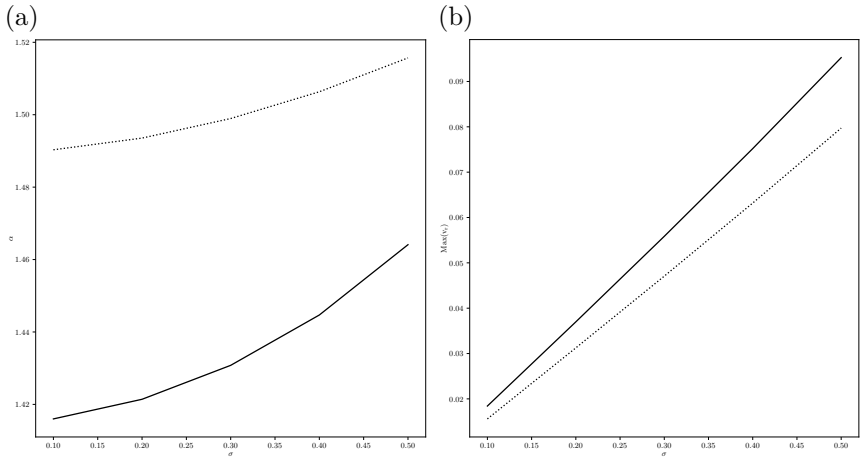

Figure 6.11.: Left: Optimization parameter as function of losses Γ/g. Right: Maximal value of the radial velocity as function of losses Γ/g. In both figures the dotted lines represent the numerical data and the straight lines the solutions obtained from the projection optimization method. Taken from [25].

7. Continuum Model

As the final chapter of thesis we consider a lattice model describing a Photon Bose-Einstein condensate introduced in reference [24]. The special feature of this model is that there is no explicit interaction term, but instead it is claimed that an effective interaction is achieved by an imaginary hopping term. The underlying equation of motion of this model is the following

$$i\hbar\frac{\partial\psi(\mathbf{x},t)}{\partial t} = -(1-i\kappa)J\sum_{\mathbf{x}'\in\mathcal{N}_{\mathbf{x}}} + V(\mathbf{x})\psi(\mathbf{x}) + \frac{i}{2}\left[B_{21}M_2(\mathbf{x}) - B_{12}M_1(\mathbf{x}) - \Gamma\right]\psi(\mathbf{x})\,, \tag{7.1}$$

where Γ denotes a loss global rate and V an external potential. Reference [24] claims that the effective interaction is modeled by the energy relaxation strength and related by the Kennard-Steppanov relation to

$$\kappa = \frac{1}{2}\beta B_{12}M_1\,, \tag{7.2}$$

where β is proportional to the inverse temperature

$$\beta = \frac{1}{k_B T}\,. \tag{7.3}$$

To provide a plausible indication for this far-reaching claim we consider the continuum model of 7.1

$$i\hbar\frac{\partial\psi(\mathbf{x},t)}{\partial t} = -\frac{\hbar^2}{2m}(1-i\kappa)\boldsymbol{\nabla}^2\psi(\mathbf{x},t) + V(\mathbf{x})\psi(\mathbf{x},t) + g\left|\psi(\mathbf{x},t)\right|^2\psi(\mathbf{x},t) + \frac{i}{2}\left[\gamma - \Gamma\left|\psi(\mathbf{x},t)\right|^2\right]\psi(\mathbf{x},t)\,, \tag{7.4}$$

where we use the relation between hopping J, the lattice length a and the kinetic energy

$$Ja^2 = \frac{\hbar^2}{2m}\,. \tag{7.5}$$

In fact this corresponds to the cGPE (2.17) with an additional imaginary kinetic term. Furthermore we specify the external trapping potential to be a harmonic trap

$$V(\mathbf{x}) = \frac{1}{2}m\omega^2\left|\mathbf{x}\right|^2\,. \tag{7.6}$$

Note that using the continuum model (7.4) we consider at first a model with two interaction terms in order to check whether the above mentioned claim of [24] is

correct. This leads at the end to a better comparison of the determined results with our previous calculations. Applying the separation ansatz

$$\psi(\mathbf{x},t) = \psi(\mathbf{x})e^{-\frac{i}{\hbar}\mu t} \tag{7.7}$$

leads to the steady state equation

$$\mu\psi(\mathbf{x},t) = -\frac{\hbar^2}{2m}\left(1-i\kappa\right)\boldsymbol{\nabla}^2\psi(\mathbf{x},t)+V(\mathbf{x})\psi(\mathbf{x},t)+g\left|\psi(\mathbf{x},t)\right|^2\psi(\mathbf{x},t)+\frac{i}{2}\left[\gamma-\Gamma\left|\psi(\mathbf{x},t)\right|^2\right]\psi(\mathbf{x},t)\,. \tag{7.8}$$

In order to apply the projection optimization method we make the ansatz for the wave function

$$\Psi(r) = \sqrt{\frac{N}{\pi q^2}}e^{-\frac{r^2}{2q^2}-iAr^2} \tag{7.9}$$

where we included three trial parameters N, q and A similar to Section 5.3. The projection optimization method applied to the ansatz (7.9) yields three projection optimization equations

$$\int_{\mathbb{R}^2} d\mathbf{r}\left\{\mathrm{EOM}\left[\Psi,\Psi^*\right](\mathbf{r})\frac{\partial\Psi^*(r)}{\partial N}+\mathrm{EOM}^*\left[\Psi,\Psi^*\right](\mathbf{r})\frac{\partial\Psi(r)}{\partial N}\right\}=0\,, \tag{7.10}$$

$$\int_{\mathbb{R}^2} d\mathbf{r}\left\{\mathrm{EOM}\left[\Psi,\Psi^*\right](\mathbf{r})\frac{\partial\Psi^*(r)}{\partial q}+\mathrm{EOM}^*\left[\Psi,\Psi^*\right](\mathbf{r})\frac{\partial\Psi(r)}{\partial q}\right\}=0\,, \tag{7.11}$$

$$\int_{\mathbb{R}^2} d\mathbf{r}\left\{\mathrm{EOM}\left[\Psi,\Psi^*\right](\mathbf{r})\frac{\partial\Psi^*(r)}{\partial A}+\mathrm{EOM}^*\left[\Psi,\Psi^*\right](\mathbf{r})\frac{\partial\Psi(r)}{\partial A}\right\}=0\,. \tag{7.12}$$

Inserting the steady-state equation of motion (7.8) and the respective derivatives of the ansatz (7.9) yields the following integrals

$$\int_0^\infty dr\Bigg\{\mu r+\frac{\hbar^2}{2m}\left[-\frac{2r}{q^2}+\frac{r^3}{q^4}-4A^2r^3\right]-\kappa\frac{\hbar^2}{2m}\left[4Ar-\frac{4Ar^3}{q^2}\right] \tag{7.13}$$

$$-\frac{m\omega^2}{2}r^3-g\frac{N}{\pi q^2}re^{-\frac{r^2}{q^2}}\Bigg\}\frac{N}{\pi q^2}e^{-\frac{r^2}{q^2}}=0\,, \tag{7.14}$$

$$\int_0^\infty dr\Bigg\{\mu r+\frac{\hbar^2}{2m}\left[-\frac{2r}{q^2}+\frac{r^3}{q^4}-4A^2r^3\right]-\kappa\frac{\hbar^2}{2m}\left[4Ar-\frac{4Ar^3}{q^2}\right] \tag{7.15}$$

$$-\frac{m\omega^2}{2}r^3-g\frac{N}{\pi q^2}e^{-\frac{r^2}{q^2}}\Bigg\}\frac{N}{\pi q^2}e^{-\frac{r^2}{q^2}}\left[\frac{r^2}{q^3}-\frac{1}{q}\right]=0\,, \tag{7.16}$$

$$\int_0^\infty dr\Bigg\{\frac{\hbar^2}{2m}\left[4Ar^3+\frac{4Ar^5}{q^2}\right]+\kappa\frac{\hbar^2}{2m}\left[-\frac{2r^3}{q^2}+\frac{r^5}{q^4}-4A^2r^5\right] \tag{7.17}$$

$$+\gamma r^3-\frac{\Gamma N r^3}{\pi q^2}e^{-\frac{r^2}{q^2}}\Bigg\}\frac{N}{\pi q^2}e^{-\frac{r^2}{q^2}}=0\,. \tag{7.18}$$

Calculating the integrals leads to three equations, one for each trial parameter

$$\mu - \frac{\hbar^2}{2mq^2} - \frac{2\hbar^2 A^2 q^2}{m} + \kappa\frac{\hbar^2 A}{2m} - \frac{m\omega^2}{2}q^2 - g\frac{N}{2\pi q^2} = 0\,, \tag{7.19}$$

$$\frac{\hbar^2}{2mq^3} - \frac{2A^2\hbar^2}{m}q + \kappa\frac{2\hbar^2 A}{mq} - \frac{m\omega^2}{2}q + \frac{gN}{4\pi q^3} = 0\,, \tag{7.20}$$

$$\frac{3\hbar^2 A}{m}q^2 - \kappa\frac{2\hbar^2 A^2}{m}q^4 + \gamma q^2 - \frac{\Gamma N}{2\pi} = 0\,. \tag{7.21}$$

By introducing the oscillator length (5.12) the equations (7.19)–(7.21) can be simplified resulting in

$$N = 2\pi\left\{\left[\frac{\mu}{g} + \kappa\frac{\hbar^2 A}{2mg}\right]q^2 - \left[\frac{2\hbar^2 A^2}{mg} + \frac{m\omega^2}{2g}\right]q^4 - \frac{\hbar^2}{2mg}\right\}\,, \tag{7.22}$$

$$q = \sqrt{\frac{2\kappa A l_{\mathrm{osc}}^2}{4A^2 l_{\mathrm{osc}}^4 + 1} + \sqrt{\left(\frac{2\kappa A l_{\mathrm{osc}}^2}{4A^2 l_{\mathrm{osc}}^4 + 1}\right)^2 + \frac{\frac{\tilde{g}N}{2\pi} + 1}{4A^2 l_{\mathrm{osc}}^4 + 1}}\,l_{\mathrm{osc}}}\,, \tag{7.23}$$

$$A = \frac{3}{4\kappa q^2}\left[1 \pm \sqrt{1 + \frac{8m\kappa}{9\hbar^2}\left[\gamma q^2 - \frac{\Gamma N}{2\pi}\right]}\right]\,. \tag{7.24}$$

Thus we obtained three coupled equations, which can be solved explicitly. However, this is not needed as our interest lies on the effect of the energy relaxation strength κ upon the width q of the Gauss profile (7.9). First we note that in the limit $\kappa \to 0$ all results from Section 5.3 can be reconstructed, although it is not directly clear that the parameter A does not diverge. To check this we expand Eq. (7.24) for small κ leading to

$$A = -\frac{m\left(\gamma q^2 - \frac{\Gamma n}{2\pi}\right)}{3\hbar^2 q^2} + \frac{2m^2\left(\gamma q^2 - \frac{\Gamma n}{2\pi}\right)^2}{27\hbar^4 q^2}\kappa + \mathcal{O}(\kappa^2)\,. \tag{7.25}$$

Now we can read off from Eq. (7.25) that also the parameter A does not diverge in this limit and remains constant. Also we notice from (7.23) that even in the limit of vanishing interaction strength g the width q is influenced by κ. The most important insight we get from these equations is that the width (7.23) of the condensate wave function is increased by the value of κ, as also shown in Fig. 7.1. And his remains to be true even in the limit $g \to 0$ by κ increased. Therefore we can conclude that the above introduced imaginary κ-term acts indeed like an interaction.

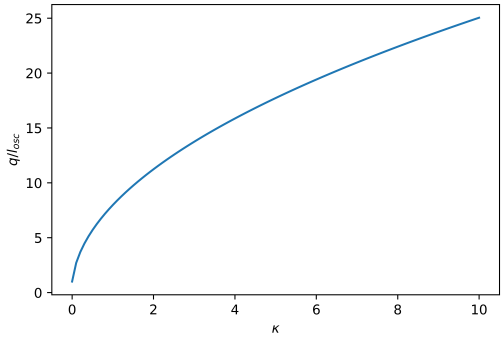

Figure 7.1.: Width q of the Gauss profile as function of the energy relaxation strength κ, plotted in units of the oscillator length l_{osc}.

8. Summary and Outlook

Inspired by numerical simulations of a single vortex described by a mean-field theory for Photon Bose-Einstein condensates in reference [24] and for nonequilibrium quantum fluids in reference [49], the aim of this thesis is to find approximate analytical solutions of the velocity field generated by a single vortex and therefore determine an analytical solution to describe the spiral shape [24].
For this purpose we start in Chapter 2 with the Gross-Pitaevskii equation (2.9) [17, 18] for closed systems and extend heuristically to a complex Gross-Pitaevskii equation (2.17) [34], which also includes the properties of an open dissipative system. Namely we add to the Gross-Pitaevskii equation an additional imaginary term describing pumping and losses of particles. Furthermore we also investigate a linear stability analysis of the complex Gross-Pitaevskii equation (2.17) and derive two eigenmodes, where the first reproduces an unstable Goldstone mode (2.36) and the second a stable eigenmode (2.37),(2.38), but with the fact that the Goldstone theorem [39] is modified.
With these two equations (2.9) and (2.17) we derive in Chapter 3 a hydrodynamic description for both a BEC in a closed and an open dissipative system. Starting with the closed system case we derive the continuity equation for the particle density (3.10), an Euler equation for the velocity field (3.13) and to have a closed description of the system also including turbulence we determine the Helmholtz vorticity equation (3.15). Afterwards we specify in the next section to a two-dimensional condensate and derive one solution for the hydrodynamic equations (3.10),(3.13) and (3.15) by introducing a stream function description of the velocity field. In the second part of Chapter 3 we then go to an open dissipative system and derive the hydrodynamic equation in this case yielding the same equations for the velocity field and the vorticity as in the closed system. The only difference appears in the continuity equation (3.31), which now has an inhomogeneous right-hand side. Also due to this nhomogeneity of the continuity equation we are not able to find, in a similar way to the closed system, a solution for the hydrodynamic equations (3.39).
To overcome this issue we construct in Chapter 4 a new projection optimization method [25], which is based on a projection of the underlying Hilbert space to a parameter manifold spanned by a set of parameters due to the choice of an ansatz wave function. With that method [25] we are then able to reduce a partial differential equation to a set of ordinary differential equations, which is in general easier to solve than the whole problem.
As a first example of the projection optimization method [25] we consider in Chapter 5 the complex Gross-Pitaevskii equation (2.17) with an external harmonic trap. By using an standard Gauss ansatz (5.2) with the particle number and the width

of the Gauss profile as optimization parameters we calculate these parameters with both the projection optimization method and the well known cumulant method [54] yielding the same results. By that inspired we even proof that the projection optimization equations and the cumulant equations are equivalent. As a second example for the projection optimization method we then finally consider a single vortex in an infinite homogeneous system in Chapter 6. To familiarise yourself with the system we have at first a closer look into the closed system case and calculate various types of ansatz functions ending with the conclusion that the simplest and also good approaching function is the standard literature ansatz (6.3). Now going to the open system case and using the standard ansatz for closed systems (6.3) we are then able to approximate the solution of the complex Gross-Pitaevskii equation (2.17) in a stationary state yielding compared with numerical simulations a good match for the density profile and an even better match for the spiraling velocity field.
As an last example and also a first calculation for future work we consider in Chapter 7 a more general equation of motion from reference [24]. In this model we are working out by considering the continuum limit of [24] how the additional imaginary term influences the particle-particle interaction. Therefore we make an Gaussian ansatz for the wave function (7.9) and apply the projection optimization method [25]. This yields that the introduced term highly influences the width of the condensate wave function and therefore can be seen similar to an interaction term.
To sum up, in this thesis we constructed a new optimization method [25], which opens the door for finding analytical approximate solutions to any systems. We then apply this new method to three different examples and yield a good match of the analytical solutions with numerical simulations.

As described above the projection optimization method [25] opens the door for further investigations in the future. A still open question is how the nonlinearities in [24] involved in pumping and dissipation can lead to a finite vortex core in absence of a contact interation term in the mean-field model. Applying the projection optimization method to the mean-field equation of [24] might give the answer. Furthermore in this thesis we show that our model is valid for small values of pumping and losses. Therefore by applying a different, much more complicated, ansatz to the projection optimization equations might solve this problem. A reasonable ansatz is similar to the closed system Pade-approxiumation derived by N. Berloff [64]. Also we can consider extending the analysis in order to determine how two vortices in an open-dissipative system are interacting in comparison with the corresponding situation in a closed system. With these results we then can investigate the consequences for the BKT transition [65–67] between bound and unbound vortex pairs, which occur also for open-dissipative systems [59].

A. Projection Optimization Method

As described in Chapter 4 the projection optimization method generalises the standard optimization method [**vm1996erez**] and the well know cumulant optimization method [13, 54] to all kinds of systems. The method is not restricted to a special kind of ansatz function like the cumulant method [13, 54] or needs particle conservation like the standard optimization method [**vm1996erez**]. Furthermore from a mathematical point of view we introduced the projection optimization method as a projection of the equation of motion onto a parameter manifold spanned by trial or optimization parameters. This trial parameters were introduced by the ansatz wave function. However, this procedure can also be interpreted geometrically. To this end we consider the following equation of motion

$$\mathrm{EOM}(\mathbf{X}) = \dot{\mathbf{X}} - \mathbf{F}(\mathbf{X}) = 0\,, \tag{A.1}$$

where $\mathbf{X}, \mathbf{F}(\mathbf{X}) \in \mathbb{R}^N$ and $\mathbf{F}(\mathbf{X})$ denotes the underlying vector field. Assuming that we can approximate the vector $\mathbf{X}$ by a vextor $\mathbf{x}(\boldsymbol{\alpha})$, which depends on a set of M trial parameters $\boldsymbol{\alpha} = (\alpha_1, ..., \alpha_M)$

$$\mathbf{X} \approx \mathbf{x}(\boldsymbol{\alpha})\,. \tag{A.2}$$

Now introducing similar to Chapter 4 the scalar product, but note that we here are using the standard Euclidean scalar product instead of the L^2 scalar product (4.14), and calculating the projection optimization equations (4.13) yielding

$$\left\langle \dot{\mathbf{x}} - \mathbf{F}(\mathbf{x}), \frac{\partial \mathbf{x}}{\partial \alpha_i} \right\rangle = 0 \; i = 1, ..., N\,. \tag{A.3}$$

To geometrical interpret this we first recognize that due to (A.2) the trajectory $\mathbf{X}(t)$ lies on the manifold spanned by $\boldsymbol{\alpha}$ and embedded in $\mathbb{R}^N$ due to $\mathbf{x}(\boldsymbol{\alpha})$, see Fig. A.1. Therefore the partial derivative $\partial\mathbf{x}/\partial\alpha_i$ corresponds to a tangential vector of the manifold and points perpendicular to $\alpha_i = const$ line, see Fig. A.1. According to [25] (A.3) projects the dynamics of (A.1) onto the manifold, which is quite natural. After projecting we therefore have, and also see in Fig. A.1, that the approximation $\mathbf{x}$ can be expanded in terms of the partial derivatives yielding

$$\mathbf{x} = \sum_{j=1}^{M} \dot{\alpha}_j \frac{\partial \mathbf{x}}{\partial \alpha_j}\,. \tag{A.4}$$

This leads now together with (A.3) to

$$\sum_{j=1}^{M} \dot{\alpha}_j g_{ji}(\boldsymbol{\alpha}) = \left\langle \mathbf{F}(\mathbf{x}), \frac{\partial \mathbf{x}}{\partial \alpha_i} \right\rangle\,, \tag{A.5}$$

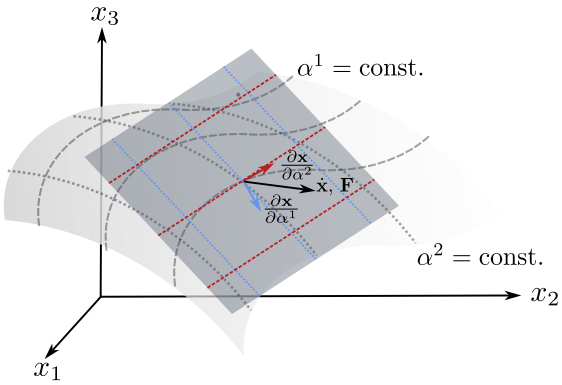

Figure A.1.: Geometrical illustration of projection optimization method for $N = 3$ and $M = 2$. Taken from [25]

where g_{ji} denotes the mentric of the manifold

$$g_{ji}(\boldsymbol{\alpha}) = \left\langle \frac{\partial \mathbf{x}}{\partial \alpha_j}, \frac{\partial \mathbf{x}}{\partial \alpha_i} \right\rangle . \tag{A.6}$$

Defining the right hand side of (A.5) as the projected components f_i of the vector field $\mathbf{F}(\mathbf{x})$ onto the manifold

$$f_i(\boldsymbol{\alpha}) = \left\langle \mathbf{F}(\mathbf{x}), \frac{\partial \mathbf{x}}{\partial \alpha_i} \right\rangle . \tag{A.7}$$

Because Eq. (A.7) holds we can interpret the vector $\mathbf{f}$ as the projection of the vector field $\mathbf{F}$ onto the manifold and is therefore the approximation of the vector field $\mathbf{F}$. Finally we get the following equations for the trial parameters

$$\dot{\boldsymbol{\alpha}} = \mathbf{f}(\boldsymbol{\alpha}) \tag{A.8}$$

as due to the projection (A.3) equations this corresponds to an approximation of the equation of motion in the manifold.

B. Useful Integrals

In this Appendix we show the calculations concerning the Section 6.1.2 in more detail. To this end we separate the following into two parts. In the first part we consider the exponential ansatz function (6.13) and then afterwards we consider the hyperbolic tangens ansatz function (6.14).

B.1. Exponential Ansatz

According to Section 6.1.2 we are considering the following integral (6.15)

$$\epsilon_V = \int_0^D dr \left\{ \beta^2 r e^{-2\beta r} + \frac{1}{r}\left(1 - e^{-\beta r}\right)^2 + \frac{r}{2}\left(1 - \left(1 - e^{-\beta r}\right)^2\right)^2 \right\} \tag{B.1}$$

This can be simplified as follows

$$0 = \int_0^D dr \left\{ r\beta^2 e^{-2\beta r} + \frac{1}{r} + \frac{1}{r}e^{-2\beta r} - \frac{2}{r}e^{-\beta r} + 2re^{-2\beta r} + \frac{r}{2}e^{-4\beta r} - 2re^{-3\beta r} \right\} \tag{B.2}$$

Therefore we have to calculate the following seven integrals

$$I_1 = \int_0^D drr\beta^2 e^{-2\beta r} = -\frac{\beta^2}{2}\frac{\partial}{\partial\beta}\int_0^D dre^{-2\beta r} = \frac{1}{4} - \frac{1}{4}e^{-2\beta D} - \frac{\beta D}{2}e^{-2\beta D} \tag{B.3}$$

$$I_2 = \int_0^D dr2re^{-2\beta r} = -\frac{\partial}{\partial\beta}\int_0^D dre^{-2\beta r} = \frac{1}{2\beta^2} - \frac{1}{2\beta^2}e^{-2\beta D} - \frac{D}{\beta}e^{-2\beta D} \tag{B.4}$$

$$I_3 = \int_0^D dr\frac{r}{2}e^{-4\beta r} = -\frac{1}{8}\frac{\partial}{\partial\beta}\int_0^D dre^{-4\beta r} = \frac{1}{32\beta^2} - \frac{1}{32\beta^2}e^{-4\beta D} - \frac{D}{8\beta}e^{-4\beta D} \tag{B.5}$$

$$I_4 = \int_0^D dr - 2re^{-3\beta r} = \frac{2}{3}\frac{\partial}{\partial\beta}\int_0^D dre^{-3\beta r} = -\frac{2}{9\beta^2} + \frac{2}{9\beta^2}e^{-3\beta D} + \frac{2D}{3\beta}e^{-3\beta D} \tag{B.6}$$

$$I_5 = \int_0^D dr\frac{1}{r} = \lim_{r_0\to 0}\int_{r_0}^D dr\frac{1}{r} = \lim_{r_0\to 0}\left\{\ln(D) - \ln(r_0)\right\} \tag{B.7}$$

$$I_6 = \int_0^D dr\frac{1}{r}e^{-2\beta r} = \lim_{r_0\to 0}\int_{2\beta r_0}^{2\beta D} dt\frac{1}{t}e^{-t} = \lim_{r_0\to 0}\left\{\Gamma(0, 2\beta r_0) - \Gamma(0, 2\beta D)\right\} \tag{B.8}$$

$$I_7 = \int_0^D dr - \frac{2}{r}e^{-\beta r} = -2\lim_{r_0\to 0}\int_{\beta r_0}^{\beta D} dt\frac{1}{t}e^{-t} \tag{B.9}$$

Note that we introduced in (B.7)–(B.9) also an additional infrared cutoff due to divergences. Furthermore we introduced the upper Gamma-function [68]

$$\Gamma(s,x) = \int_d tx^{\infty} t^{s-1} e^{-t} \,. \tag{B.10}$$

Notice that the integrals (B.7)–(B.9) diverge separately, but by considering the sum and two different expansion formulas for the upper Gamma function, one for small x [68]

$$\Gamma(0,x) = -\gamma - \ln(x) - \sum_{k=1}^{\infty} \frac{(-x)^k}{k(k!)} \,, \tag{B.11}$$

where γ denotes the Euler-Mascheroni constant and for for large x [69]

$$\Gamma(0,x) = \frac{e^{-x}}{x} \sum_{k=1}^{n} \frac{(-1)^k k!}{x^k} \,, \text{ where } n \text{ is large enough} \tag{B.12}$$

we see that all divergences vanish automatically

$$I_5 + I_6 + I_7 = \ln\left(\frac{\beta D}{2}\right) + \gamma - e^{-2\beta D} \sum_{k=0}^{n} \frac{(-1)^k k!}{(2\beta D)^{k+1}} + 2e^{-\beta D} \sum_{k=0} n \frac{(-1)^k k!}{(\beta D)^{k+1}} \,. \tag{B.13}$$

From Eq. (B.13) we see that except of the logarithmic divergence all other divergences vanish. Therefore by taking the derivative with respect to β we don't have any divergences left.

B.2. Hyperbolic Tangens Ansatz

According to Section 6.1.2 we are considering the following integral (6.18)

$$\epsilon_V = \int_0^D dr \left\{ r\delta \left[1 - \tanh^2(\delta r)\right] + \frac{\tanh^2(\delta r)}{r} + \frac{r}{2} \left[1 - \tanh^2(\delta r)\right]^2 \right\} . \tag{B.14}$$

After rewriting (B.14) this leads to the following six integrals, of which the five can mostly be calculated by using partial integration and identities for hyperbolic

tangens

$$S_1 = \int_0^D dr \left\{ r\delta + \frac{r}{2} \right\} = \frac{1}{2}\delta D^2 + \frac{1}{4}D^2 \,, \tag{B.15}$$

$$S_2 = \int_0^D dr\delta r \tanh^4(\delta r) = \frac{1}{2}\delta D^2 - D\tanh(\delta D) - \frac{1}{3}D\tanh^3(\delta D) \tag{B.16}$$

$$+ \frac{4}{3\delta}\ln(\cosh(\delta D)) + \frac{1}{6\delta\cosh^2(\delta D)} + \frac{1}{6\delta} \,, \tag{B.17}$$

$$S_3 = \int_0^D dr\frac{r}{2}\tanh^4(\delta r) = \frac{1}{4}D^2 - \frac{D}{2\delta}\tanh(\delta D) - \frac{D}{6\delta}\tanh^3(\delta D) \tag{B.18}$$

$$+ \frac{2}{3\delta^2}\ln(\cosh(\delta D)) + \frac{1}{12\delta^2\cosh^2(\delta D)} + \frac{1}{12\delta^2} \,, \tag{B.19}$$

$$S_4 = -2\int_0^D dr\delta r\tanh^2(\delta r) = -\delta D^2 - 2D\tanh(\delta D) - \frac{2}{\delta}\ln(\cosh(\delta D)) \tag{B.20}$$

$$S_5 = -2\int_0^D dr\frac{r}{2}\tanh^2(\delta r) = -\frac{1}{2}D^2 + \frac{D}{\delta}\tanh(\delta D) - \frac{1}{\delta^2}\ln(\cosh(\delta D)) \,. \tag{B.21}$$

The last integral is, however, much more complicated as needs a special treatment. First we note that it holds

$$\tanh(x) = 1 - \frac{2}{e^{2x}+1} \,. \tag{B.22}$$

With this we can make the first step in calculating the last remaining integral

$$S_6 = \int_0^D dr\frac{1}{r}\tanh^2(\delta r) = \int_0^{\delta D} dx\frac{1}{x}\tanh^2(x) = \int_0^1 dx\frac{1}{x}\tanh^2(x) + \int_1^{\delta D} dx\frac{1}{x}\tanh^2(x) \tag{B.23}$$

$$= \int_0^1 dx\frac{1}{x}\tanh(x) + \int_1^{\delta D} dx\left\{ \frac{1}{x} + \frac{4}{x\left(e^{2x}+1\right)^2} - \frac{4}{x\left(e^{2x}+1\right)} \right\} \tag{B.24}$$

$$= \int_0^1 dx\frac{1}{x}\tanh(x) + \ln(\delta D) + \int_1^{\infty} dx\left\{ \frac{4}{x\left(e^{2x}+1\right)^2} - \frac{4}{x\left(e^{2x}+1\right)} \right\} \tag{B.25}$$

$$- \int_{\delta D}^{\infty} dx\left\{ \frac{4}{x\left(e^{2x}+1\right)^2} - \frac{4}{x\left(e^{2x}+1\right)} \right\} \tag{B.26}$$

By substituting $y = 1/x$ in the second integral allows to combine this with the first integral resulting in

$$S_6 = \int_0^1 dx\left\{ \frac{\tanh(x)}{x} + \frac{4}{x\left(e^{2x}+1\right)^2} - \frac{4}{x\left(e^{2x}+1\right)} \right\} \tag{B.27}$$

$$- \int_{\delta D}^{\infty} dx\left\{ \frac{4}{x\left(e^{2x}+1\right)^2} - \frac{4}{x\left(e^{2x}+1\right)} \right\} + \ln(\delta D) \tag{B.28}$$

Now we note that the first integral can not be solved analytically, however, a numerical integration yields

$$\int_0^1 dx \left\{ \frac{\tanh(x)}{x} + \frac{4}{x\left(e^{2x}+1\right)^2} - \frac{4}{x\left(e^{2x}+1\right)} \right\} = R \approx 0.2095\,, \tag{B.29}$$

whereas the second integral converges in the limit $D \to \infty$ to zero. Therefore considering large D this integral does not influence the value of the integral.

$$\int_{\delta D}^{\infty} dx \left\{ \frac{4}{x\left(e^{2x}+1\right)^2} - \frac{4}{x\left(e^{2x}+1\right)} \right\} \approx 0 \tag{B.30}$$

Therefore the last integral can be approximated by

$$S_6 \approx R + \ln(\delta D) \tag{B.31}$$

Bibliography

[1] A. Einstein, "Sitzungsberichte der Preussischen Akademie der Wissenschaften", Physikalisch-Mathematische Klasse **261**, 1925 (1924).

[2] S. N. Bose, "Plancks Gesetz und Lichtquantenhypothese", Zeitschrift für Physik **26**, 178 (1924).

[3] J. F. Allen and A. Misener, "Flow of Liquid Helium II", Nature **141**, 75 (1938).

[4] F. London, "On the Bose-Einstein Condensation", Physical Review **54**, 947 (1938).

[5] L. Pitaevskii and S. Stringari, *Bose-Einstein Condensation and Superfluidity*, Vol. 164 (Oxford University Press, 2016).

[6] M. H. Anderson, J. R. Ensher, M. R. Matthews, C. E. Wieman, and E. A. Cornell, "Observation of Bose-Einstein Condensation in a Dilute Atomic Vapor", science **269**, 198 (1995).

[7] K. B. Davis, M.-O. Mewes, M. R. Andrews, N. J. van Druten, D. S. Durfee, D. Kurn, and W. Ketterle, "Bose-Einstein Condensation in a Gas of Sodium Atoms", Physical review letters **75**, 3969 (1995).

[8] W. Ketterle, "Nobel lecture: When Atoms behave as Waves: Bose-Einstein Condensation and the Atom Laser", Reviews of Modern Physics **74**, 1131 (2002).

[9] J. Kasprzak, M. Richard, S. Kundermann, A. Baas, P. Jeambrun, J. M. J. Keeling, F. Marchetti, M. Szymaska, R. André, J. Staehli, et al., "Bose–Einstein condensation of exciton polaritons", Nature **443**, 409 (2006).

[10] H. Deng, H. Haug, and Y. Yamamoto, "Exciton-Polariton Bose-Einstein Condensation", Reviews of modern physics **82**, 1489 (2010).

[11] I. Carusotto and C. Ciuti, "Quantum Fluids of Light", Reviews of Modern Physics **85**, 299 (2013).

[12] J. Klaers, J. Schmitt, F. Vewinger, and M. Weitz, "Bose–Einstein Condensation of Photons in an Optical Microcavity", Nature **468**, 545 (2010).

[13] E. Stein and A. Pelster, "Open-Dissipative Mean-Field Theory for Photon Bose–Einstein Condensates" (2018).

[14] J. Klärs, "Bose-Einstein-Kondensation von paraxialem Licht", PhD thesis (Universitäts- und Landesbibliothek Bonn, 2011).

[15] J. Klaers, J. Schmitt, T. Damm, F. Vewinger, and M. Weitz, "Bose–Einstein Condensation of Paraxial Light", Applied Physics B **105**, 17 (2011).

[16] M. Wouters and I. Carusotto, "Excitations in a nonequilibrium Bose-Einstein condensate of exciton polaritons", Physical review letters **99**, 140402 (2007).

[17] L. P. Pitaevskii, "Vortex Lines in an imperfect Bose Gas", Sov. Phys. JETP **13**, 451 (1961).

[18] E. P. Gross, "Structure of a Quantized Vortex in Boson Systems", Il Nuovo Cimento (1955-1965) **20**, 454 (1961).

[19] C. Burghard Lietmeyer and J. Kroha, "Interactions of a Photon Bose-Einstein Condensate in a Dye-Filled Cavity Modelled with a Gross-Pitaevskii Equation" (2021).

[20] R. K. Smith, *Lectures on Tropical Cyclones*, 2006.

[21] W. Vinen, "Detection of single quanta of circulation in rotating helium II", Nature **181**, 1524 (1958).

[22] M. R. Matthews, B. P. Anderson, P. Haljan, D. Hall, C. Wieman, and E. A. Cornell, "Vortices in a Bose-Einstein condensate", Physical Review Letters **83**, 2498 (1999).

[23] K. W. Madison, F. Chevy, W. Wohlleben, and J. Dalibard, "Vortex formation in a stirred Bose-Einstein condensate", Physical review letters **84**, 806 (2000).

[24] V. N. Gladilin and M. Wouters, "Vortices in Nonequilibrium Photon Condensates", Physical Review Letters **125**, 215301 (2020).

[25] J. KrauSS, M. A. G. dos Santos Filho, F. E. A. dos Santos, and A. Pelster, "Projection Optimization Method for Open-Dissipative Quantum Fluids and its Application to a Single Vortex in a Photon Bose-Einstein Condensate", arXiv: 2311.10027 (2023).

[26] F. Schwabl, *Statistische Mechanik*, 2006.

[27] M. Szymanska, J. Keeling, and P. Littlewood, "Nonequilibrium quantum condensation in an incoherently pumped dissipative system", Physical review letters **96**, 230602 (2006).

[28] G. Barontini, R. Labouvie, F. Stubenrauch, A. Vogler, V. Guarrera, and H. Ott, "Controlling the dynamics of an open many-body quantum system with localized dissipation", Physical review letters **110**, 035302 (2013).

[29] O. Penrose and L. Onsager, "Bose-Einstein condensation and liquid helium", Physical Review **104**, 576 (1956).

[30] D. Werner, *Funktionalanalysis* (Springer-Verlag, 2006).

[31] J. Tempere, *Bose-Einstein Condensation, Superfluidity and Superconductivity*, 2019.

[32] W. Greiner and J. Reinhardt, *Field Quantization* (Springer Science & Business Media, 1996).

[33] N. N. Bogolyubov, "On the theory of superfluidity", J.Phys.(USSR) **11**, 14 (1947).

[34] J. Keeling and N. G. Berloff, "Spontaneous Rotating Vortex Lattices in a Pumped Decaying Condensate", Physical review letters **100**, 250401 (2008).

[35] H. Wagner, "Long-wavelength excitations and the Goldstone theorem in many-particle systems with broken symmetries", Zeitschrift für Physik **195**, 273 (1966).

[36] N. D. Mermin and H. Wagner, "Absence of ferromagnetism or antiferromagnetism in one-or two-dimensional isotropic Heisenberg models", Physical Review Letters **17**, 1133 (1966).

[37] P. C. Hohenberg, "Existence of long-range order in one and two dimensions", Physical Review **158**, 383 (1967).

[38] C. J. Pethick and H. Smith, *Bose–Einstein Condensation in Dilute Gases*, Vol. second edition (Cambridge university press, 2008).

[39] J. Goldstone, A. Salam, and S. Weinberg, "Broken Symmetries", Physical Review **127**, 965 (1962).

[40] P. K. Kundu, I. M. Cohen, and D. R. Dowling, *Fluid Mechanics* (Academic press, 2015).

[41] A. Gathmann, *Grundlagen der Mathematik, Vorlesungsskript TU Kaiserslautern (2018/19)*.

[42] L. Onsager, "Statistical Hydrodynamics", Il Nuovo Cimento (1943-1954) **6**, 279 (1949).

[43] R. Feynman, "Progress in low temperature physics", (1955).

[44] H. Lamb, *Hydrodynamics* (University Press, 1924).

[45] L. D. Landau and E. Lifshitz, *Hydrodynamik, Lehrbuch der theoretischen physik*, Vol. 5 (1991), p. 683.

[46] L. C. Evans, *Partial Differential Equations*, Vol. 19 (American Mathematical Society, 2022).

[47] X. Ma, Y. V. Kartashov, T. Gao, L. Torner, and S. Schumacher, "Spiraling vortices in exciton-polariton condensates", Physical Review B **102**, 045309 (2020).

[48] N. G. Berloff, "Turbulence in exciton-polariton condensates", arXiv preprint arXiv:1010.5225 (2010).

[49] V. N. Gladilin and M. Wouters, "Interaction and motion of vortices in nonequilibrium quantum fluids", New Journal of Physics **19**, 105005 (2017).

[50] K. G. Lagoudakis, M. Wouters, M. Richard, A. Baas, I. Carusotto, R. André, L. S. Dang, and B. Deveaud-Plédran, "Quantized vortices in an exciton–polariton condensate", Nature physics **4**, 706 (2008).

[51] H. Helmholtz, "Über Integrale der hydrodynamischen Gleichungen, welche den Wirbelbewegungen entsprechen.", Journal für die reine und angewandte Mathematik **1858**, 25 (1858).

[52] C. Surulescu, *Partial Differential Equations: An Introduction.*

[53] E. Stein, F. Vewinger, and A. Pelster, "Collective modes of a photon Bose–Einstein condensate with thermo-optic interaction", New Journal of Physics **21**, 103044 (2019).

[54] N. Mann, M. R. Bakhtiari, A. Pelster, and M. Thorwart, "Nonequilibrium quantum phase transition in a hybrid atom-optomechanical system", Physical review letters **120**, 063605 (2018).

[55] V. M. Pérez-García, M. A. Porras, and L. Vázquez, "The nonlinear schrödinger equation with dissipation and the moment method", en, Physics Letters A **202**, 176 (1995).

[56] F. Riesz and B. S. Nagy, "Über Kontraktionen des Hilbertschen Raumes", Acta Univ. Szeged. Sect. Sci. Math **10**, 202 (1943).

[57] M. Reed and B. Simon, *I: Functional analysis*, Vol. 1 (Academic press, 1981).

[58] J. Kierzenka and L. F. Shampine, "A bvp solver based on residual control and the Matlab PSE", ACM Transactions on the Mathematical Software (TOMS) **27**, 299 (2001).

[59] V. N. Gladilin and M. Wouters, "Vortex unbinding transition in nonequilibrium photon condensates", Physical Review A **104**, 043516 (2021).

[60] J. Prüss, M. Wilke, and M. Wilke, *Gewöhnliche Differentialgleichungen und dynamische systeme* (Springer, 2010).

[61] M. Kobayashi, P. Parnaudeau, F. Luddens, C. Lothodé, L. Danaila, M. Brachet, and I. Danaila, "Quantum turbulence simulations using the Gross–Pitaevskii equation: high-performance computing and new numerical benchmarks", Computer Physics Communications **258**, 107579 (2021).

[62] W. Bao and D. Jaksch, "An explicit unconditionally stable numerical method for solving damped nonlinear Schrödinger equations with a focusing nonlinearity", SIAM Journal on Numerical Analysis **41**, 1406 (2003).

[63] G. R. Dennis, J. J. Hope, and M. T. Johnsson, "XMDS2: Fast, scalable simulation of coupled stochastic partial differential equations", Computer Physics Communications **184**, 201 (2013).

[64] N. G. Berloff, "Padé approximations of solitary wave solutions of the Gross–Pitaevskii equation", Journal of Physics A: Mathematical and General **37**, 1617 (2004).

[65] V. Berezinskii, "Destruction of long-range order in one-dimensional and two-dimensional systems having a continuous symmetry group I. Classical systems", Sov. Phys. JETP **32**, 493 (1971).

[66] V. Berezinskii, "Destruction of long-range order in one-dimensional and two-dimensional systems possessing a continuous symmetry group. II. Quantum systems", Sov. Phys. JETP **34**, 610 (1972).

[67] J. M. Kosterlitz and D. J. Thouless, "Ordering, metastability and phase transitions in two-dimensional systems", in *Basic notions of condensed matter physics* (CRC Press, 1973), pp. 493–515.

[68] I. Gradsteyn, "S and ryzhik im 1965", Tables ofhtegrals, Series and Products.

[69] E. Masina, "Useful review on the Exponential-Integral special function", arXiv preprint arXiv:1907.12373 (2019).

Acknowledgements

At the end of my physics degree and the five and a half years associated with it, I would like to thank a few very special people. My biggest thanks go to my parents, who have supported me unconditionally in every situation. In particular, I would like to thank my father for the many hours we spent studying together. My next thanks go to my supervisor Priv.-Doz. Dr Axel Pelster for the opportunity to be part of a research project and who was always on hand with help and advice. Next, I would like to thank my fellow students, with whom it was always fun and who were always on hand to give me advice. In particular, I would like to thank Pascal Jung and Paul Beckermann. Last but not least, I would also like to thank Marcos Alberto Gonçalves dos Santos Filho for his active support while I was working on my thesis and, of course, for the many great conversations I had outside of physics topics.

Selbstständigkeitserklärung

Hiermit erkläre ich, dass ich die vorliegende Arbeit selbstständig verfasst und alle verwendeten Quellen als solche gekennzeichnet habe.

Kaiserslautern, 05.12.2023 J. Krauß

Ort, Datum Joshua Krauß

Fachbereich Physik

Rheinland-Pfälzische Technische
Universität Kaiserslautern Landau

Postfach 3049
67653 Kaiserslautern, Germany

www.physik.rptu.de/

Rheinland-Pfälzische
Technische Universität
Kaiserslautern
Landau